



## TOPICAL REVIEW

## 2D tribotronic transistors

## OPEN ACCESS

RECEIVED  
28 July 2022REVISED  
9 October 2022ACCEPTED FOR PUBLICATION  
1 November 2022PUBLISHED  
24 November 2022

Original content from  
this work may be used  
under the terms of the  
[Creative Commons  
Attribution 4.0 licence](#).

Any further distribution  
of this work must  
maintain attribution to  
the author(s) and the title  
of the work, journal  
citation and DOI.

Ziwei Huo<sup>1,2</sup>, Jinran Yu<sup>1,2</sup> , Yonghai Li<sup>1,3</sup>, Zhong Lin Wang<sup>1,2,4,\*</sup> and Qijun Sun<sup>1,2,3,5,\*</sup> <sup>1</sup> Beijing Institute of Nanoenergy and Nanosystems, Chinese Academy of Sciences, Beijing 101400, People's Republic of China<sup>2</sup> School of Nanoscience and Technology, University of Chinese Academy of Sciences, Beijing 100049, People's Republic of China<sup>3</sup> Center on Nanoenergy Research, School of Physical Science and Technology, Guangxi University, Nanning 530004, People's Republic of China<sup>4</sup> School of Materials Science and Engineering, Georgia Institute of Technology, Atlanta, GA 30332-0245, United States of America<sup>5</sup> Shandong Zhongke Naneng Energy Technology Co., Ltd, Dongying 257061, People's Republic of China

\* Authors to whom any correspondence should be addressed.

E-mail: [zhong.wang@mse.gatech.edu](mailto:zhong.wang@mse.gatech.edu) and [sunqijun@binn.cas.cn](mailto:sunqijun@binn.cas.cn)**Keywords:** 2D materials, tribotronics, field effect transistor, triboelectric nanogenerator, triboelectric potential**Abstract**

Since the discovery of graphene, two-dimensional (2D) materials have been widely applied to field-effect transistors due to their great potential in optoelectronics, photodetectors, intelligent sensors, and neuromorphic devices. By integrating a 2D transistor with a triboelectric nanogenerator (TENG) into a tribotronic transistor, the induced triboelectric potential can readily regulate the charge carrier transport characteristics in the semiconductor channel. The emerging research field of tribotronics (mainly tribotronic transistors) has attracted extensive attention due to their significant applications in various sensation and human–machine interactions. Here, this review summarizes the recent developments of 2D tribotronic transistors. Firstly, the electrical, optoelectronic, and piezoelectric properties of typical 2D materials are introduced. Then, tribotronic tuning at the micro/nanoscale is discussed together with the methodologies of thermionic emission, triboelectricity tunneling, and atomic force microscope probe scanning, which is of great significance for the investigation of the underlying mechanism of the tribotronic effect. In addition, macroscale tribotronic regulation via TENG mechanical displacement is discussed in detail to explore the applications of 2D tribotronic transistors in intelligent sensors, logic devices, memory devices, and artificial synapses. Finally, the challenges and perspectives for 2D tribotronic transistors are discussed.

**1. Introduction**

Since the discovery of graphene (Gr), two-dimensional (2D) layered nanomaterials with similar structures have attracted wider attention in various research fields. The related research on the optical, electrical, mechanical, and catalytic properties of 2D transition metal dichalcogenides (TMDs) remained in the preliminary stages until critical breakthroughs that were made in recent years [1–4]. The TMDs contain 44 compounds capable of forming stable 2D structures, including metals (NbTe, TaTe, etc), semiconductors (MoS, MoSe, WS, etc), and superconductors (NbS, NbSe, TaS, etc) [5–8]. Similar to Gr, TMDs are layered materials that can be exfoliated to obtain monolayer structures. Among them, MoS<sub>2</sub> is the most profoundly investigated material due to its potential application in electronics and optoelectronics, and other 2D materials, such as the MXene, hexagonal boron nitride (h-BN), and main group metal dichalcogenides (SnSe, SnS, ZnS, etc), attract the interest of researchers due to their excellent properties [9–11]. The 2D materials have great potential in the future semiconductor industry because of their abundant and unique physical properties, and the transport properties of the electronic devices based on these 2D materials under ambient environment conditions are the basis for the development of the semiconductor industry.

Since the world's first nanogenerator (NG) device was proposed in 2006, various NG-based devices have been applied in interdisciplinary research fields [12]. In 2012, Fan *et al* innovatively proposed a triboelectric

nanogenerator (TENG) based on contact electrification (or triboelectrification) between two different materials [13]. Due to the benefits of harvesting low-frequency and high-entropy (bio)mechanical energy from the surrounding environment, TENGs have made great achievements following the technology Roadmap for supplying micro/nano energy, self-powering diversified sensory systems, working as high-voltage power sources, scavenging from water/sea waves (i.e. blue energy), and inspiring interfacial spectroscopy [14, 15]. The TENG offers novel self-powered nanotechnology by relying on the unique way to scavenge energy from the human body or external circumstances and supplying it to portable electronics and micro/nanodevices, which has laid both the theoretical and practical foundations for the realization of self-powered systems, tribotronic devices, and the energy-autonomy Internet of Things (IoTs) [16–18].

The field effect transistor (FET) is a significant milestone in the semiconductor industry, which performs with high input impedance, low noise, good thermal stability, and is a simple process [19–21]. Moreover, it is widely applied to electronic devices, large-scale integrated circuits, human–computer interaction, and other related fields. With regard to device engineering, the transistor gate can be readily extended for sensation/modulation by elongating the electrode length, augmenting with a dual-gate or a split-gate, or integrating with functional components [22]. With the continuous development of the IoTs and the sensory network, electronic devices are gradually being miniaturized and becoming intelligent. By integrating small electronic devices into intelligent systems, a wide range of applications in the fields of human–computer interaction and environmental monitoring of the IoTs can be achieved [23]. However, a huge number of electronic devices brings the problem of a power supply with limited battery life. More importantly, it is also necessary to establish a direct interaction mechanism between electronic devices and the external environment. Commonly, traditional gate voltage regulation requires a continuous external power supply. In contrast, integration of a TENG component can realize the regulation of an FET only by relying on the triboelectric potential generated by the interaction of the friction layers in the device, which can reduce the energy consumption to a certain extent and solve the problem of the power supply. Furthermore, using a TENG to replace the traditional gate voltage for mechanical regulation can also realize better interaction between the external environment and the device. In 2014, Zhang *et al* originally applied an electrostatic potential (generated by contact electrification via a TENG unit) as the gate signal to regulate the electronic transport characteristics in a semiconductor channel [24]. Since then, the new research field of tribotronics (mainly tribotronic transistors) has received considerable attention for various sensing and human–machine interactive applications, such as logic circuits [25], smart touch switches [26], photoelectric detectors [27], and electronic skins. By integrating typical 2D materials with a tribotronic transistor, Zhao *et al* proposed the novel monolayer MoS<sub>2</sub> FET and photodetectors based on the periodically TENG-driven gate modulation, which controls the transport of the MoS<sub>2</sub> carriers to obtain a large current on/off ratio [28]. Zhang *et al* reported a tactile sensing system based on tribotronic plasma-controlled Gr FETs, which is expected to promote the development of artificial synapses and intelligent sensing [29]. These kinds of devices can retrospectively be related to the counterpart of the piezoelectric potential powered FET based on the combination of an ion-gel-gated Gr transistor and piezoelectric NGs [30], which can be considered as the first NG-driven 2D transistor. Following this, TENG-driven 2D transistors with excellent properties have been extensively investigated with more profound meanings in the family of tribotronics [31, 32]. The regulation of FETs by a triboelectric potential generated by low-frequency and intermittent mechanical displacements in TENGs is highly desirable in wearable electronic devices, sensors, memories, logic devices, artificial synapses, etc, currently rendering low requirements for high speed and miniaturization. However, high-speed operation and miniaturization have always been the research goals and future development directions of tribotronic transistors, and it is believed that they can be successfully realized in the future.

This article delivers a comprehensive review on the recent developments of 2D tribotronic transistors. Firstly, the electrical, optoelectronic, and piezoelectric properties of typical 2D materials are introduced. Then, triboelectric tuning at the nanoscale is of great significance in the investigation of 2D tribotronic transistors, and includes methodologies such as thermionic emission, tunneling triboelectricity, and atomic force microscope (AFM) probe scanning. Moreover, macroscale triboelectric regulation in conventional FETs and ion-controlled transistors via TENG mechanical displacement is also discussed in detail. In addition, the applications of 2D tribotronic transistors in this review are mainly divided into intelligent sensors, logic devices, memory devices, and artificial synapses (figure 1). Finally, the challenges and future directions for 2D tribotronic transistors are discussed. The perspectives on the challenges and possible scientific breakthroughs in the field of 2D tribotronic transistors are also proposed.

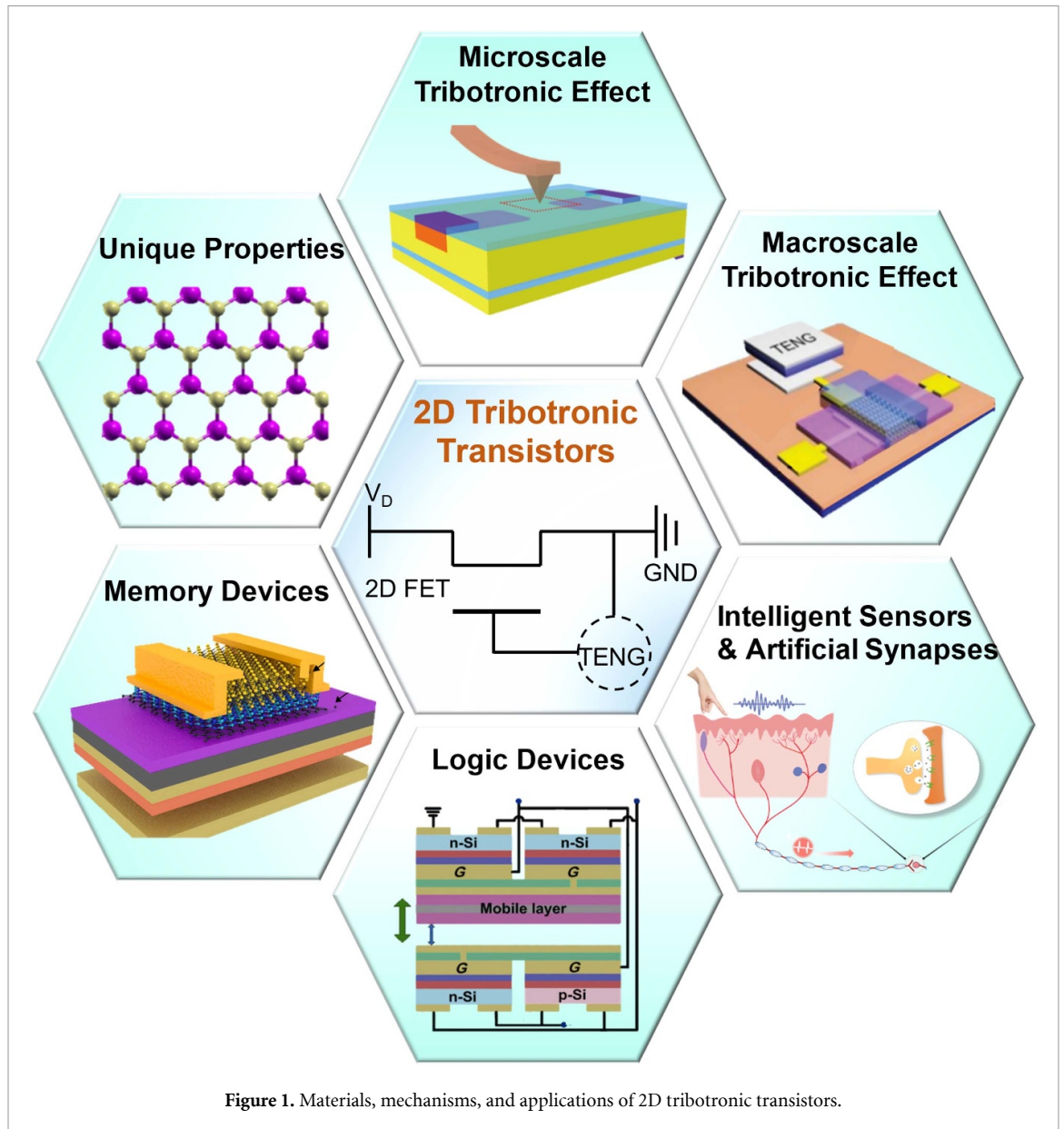
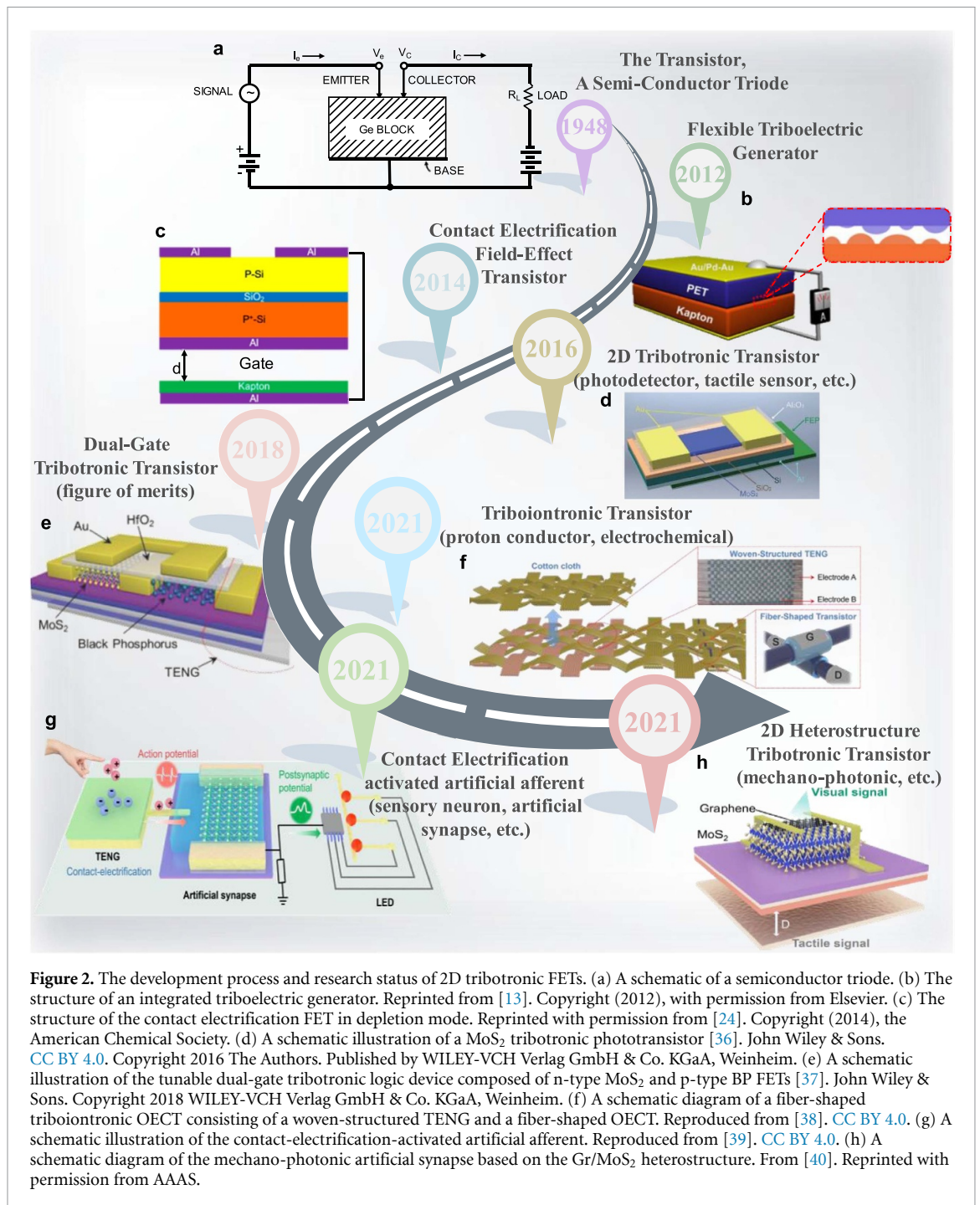


Figure 1. Materials, mechanisms, and applications of 2D tribotronic transistors.

## 2. The development history and research status of 2D tribotronic transistors

The greatest achievement of the modern electronic computer era is the invention of the ‘semiconductor transistor’, which has detonated the shock wave of the global semiconductor electronics industry and greatly improved modern electronic computers from the first to the second generation. As shown in figure 2(a), the point-contact transistor made of a Ge semiconductor and published by Bell Labs in 1948 marked the birth of the world’s first transistor [33], opening the gate for the transistor era. Due to the poor performance of point-contact transistors, Shockley proposed a bipolar transistor using p-n junctions a month later. The FET has a three-terminal structure and requires an externally supplied gate voltage to control the drain and source, which utilizes an electric field to modulate/control the transport of charge carriers in the semiconductor material [34]. The birth of the transistor has greatly changed the global historical progress of computers and other important electronic products, which is the foundation of modern information society. Since the TENG was proposed in 2012 (figure 2(b)), its development has attracted extensive attention from researchers [13]. Relying on the triboelectrification between different materials, TENG devices can readily convert mechanical energy into electrical energy to drive small electronic devices, thus exhibiting sophisticated applications in self-powered systems, such as in environmental monitoring and medical science [35]. In 2014, Zhang *et al* first proposed to use the potential difference between TENG friction materials as a gate signal to tune/control the carrier transport characteristics in FETs (figure 2(c)), and the effect was the same as the applied conventional gate voltage [24]. Based on the proposed triboelectric potential gated



transistors (i.e. tribotronic transistors), researchers have found that 2D materials with unique properties can significantly improve the performance of tribotronic transistors. In 2016, Pang *et al* first proposed a MoS<sub>2</sub>-based tribotronic phototransistor [36], extending tribotronics to the field of photodetection based on 2D materials (figure 2(d)). Subsequently, scientists have tried to diversify the application of tribotronic transistors to different research fields. For instance, Gao *et al* proposed a tunable tribotronic dual-gate FET based on a sliding-mode TENG in 2018 [37], and found that different logic states could be effectively realized by controlling the sliding displacement of the TENG (figure 2(e)). In addition to conventional tribotronic FETs, Yu *et al* proposed organic electrochemical FETs (OECTs) by utilizing electrolyte dielectrics to effectively tune the transport properties in semiconductor devices [38]. The tuning of FETs with the triboelectric potential from the fiber-woven structure of the TENG shows great potential in smart self-powered electronic textiles (figure 2(f)). Furthermore, the development of self-powered bionic electronics and intelligent interactive devices has gradually attracted widespread attention. Yu *et al* proposed that artificial afferents activated by contact electrification at the femtojoule level can identify the spatiotemporal information of touch patterns, establish dynamic logic, and identify the frequency/amplitude

**Table 1.** Tribotronic transistors based on different types of channel materials.

References	Types of 2D Materials	2D Materials	Applications
[42]	Gr	Gr	Electronic skin
[43]	Gr	Gr	Tactile sensor
[44]	TMDs	MoS <sub>2</sub>	Tactile switch
[45]	MDCs	InSe	Smart touch
[46]	Heterojunction	Gr/h-BN/MoS <sub>2</sub>	Memory device
Other types of tribotronic FETs			
References	Types of Tribotronic FETs	Channel Materials	Applications
[47]	Organic tribotronic FET	P3HT nanowires (NWs)	Tactile sensor
[31]	Organic tribotronic FET	poly (methyl methacrylate) (PMMA)/Cytosol	Pressure/magnetic sensor
[41]	Dual-gate IGZO transistor	IGZO	Multipurpose sensor

of external actions (figure 2(g)) [39]. To develop a multifunctional artificial nervous system, Yu *et al* further proposed a bioinspired mechano-photonic artificial synapse by integrating a Gr/MoS<sub>2</sub> heterojunction transistor and a TENG component (figure 2(h)) [40]. Mechano-photonic artificial synapses show great promise in realizing mixed-mode interactions, simulating complex biological nervous systems, and facilitating the development of interactive artificial intelligence. So far, other 2D materials (e.g. Gr, h-BN, WSe<sub>2</sub>) have also been demonstrated in tribotronic transistors and have exhibited great potentials in the applications of artificial synapses, memories, and logic devices.

There have been attempts to fabricate tribotronic transistors from different materials and to develop them for use in a wide variety of applications. Different kinds of 2D materials with excellent properties (Gr, TMDs, metal dichalcogenides (MDCs), heterojunctions, etc) have been demonstrated for use in tribotronic transistors. In addition to 2D materials, researchers have explored organic semiconductors, metal oxides, etc as channel materials for triboelectric FETs to achieve the desired results [41]. Table 1 shows different types of 2D materials, organic semiconductors, and metal oxides as the channel materials for tribotronic transistors and their corresponding applications.

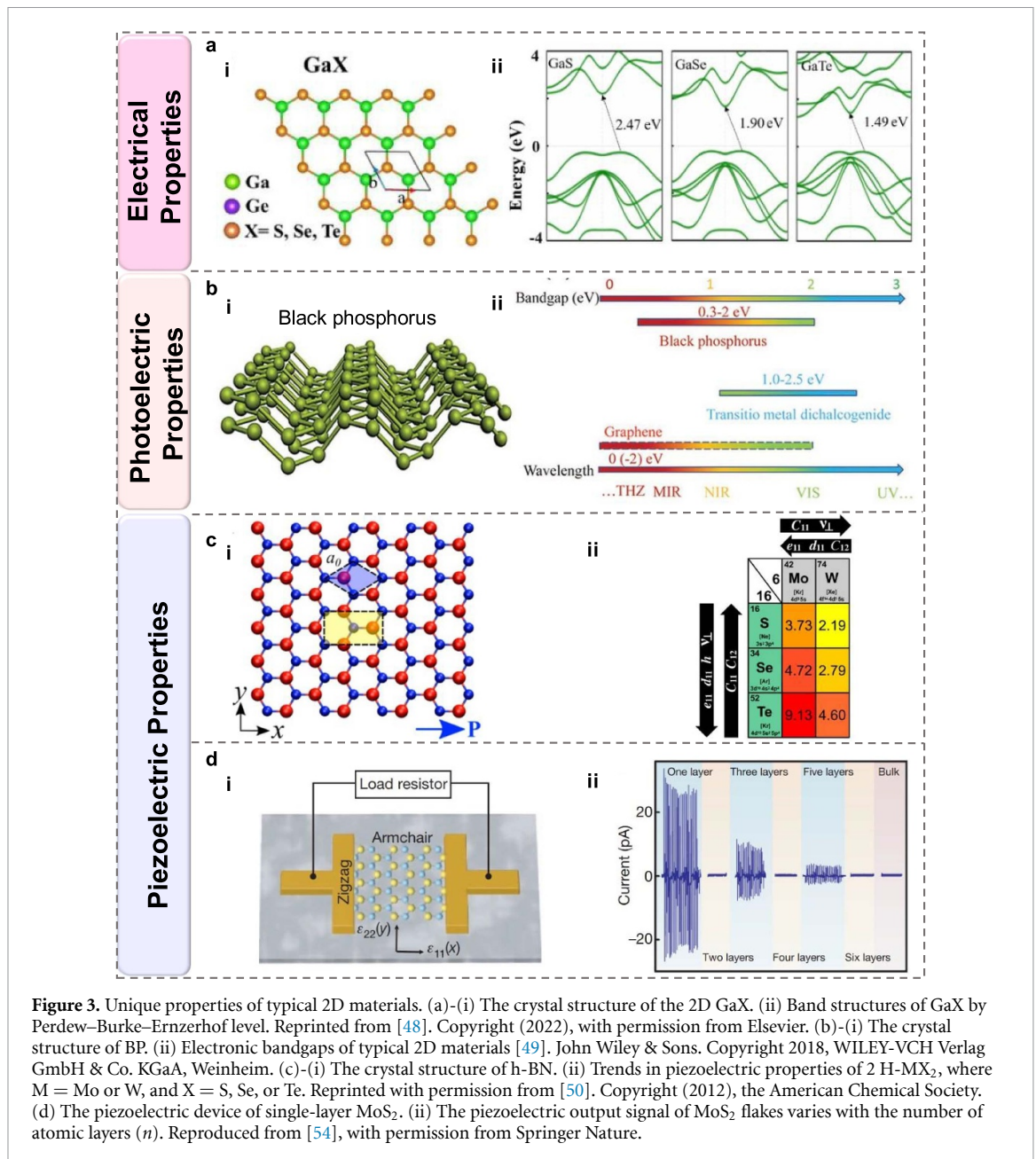
### 3. Materials and mechanism for 2D tribotronic transistors

#### 3.1. Unique 2D materials for tribotronic FETs

The 2D materials with a thickness of only one or a few atomic layers have ideal electrical, optical, and piezoelectric properties, and expand their application prospects in electronics, sensing, and energy storage and conversion. The structure of the 2D GaX and InX (X is a chalcogen, such as S, Se, or Te) is hexagonal [48], and each layer can be regarded as a bilayer of metals interposed between the two layers of chalcogens (figure 3(a)-(i)). All GaX are indirect bandgaps with specific values at 2.47, 1.90, or 1.49 eV (figure 3(a)-(ii)). This material forms a ‘Mexican cap’ band structure at the top of the valence band, resulting in a high-density electronic state. Among them, InSe has more excellent electrical properties than Si, which is generally used in modern electronic products. Moreover, the ultrathin InSe has a large energy gap, allowing the FETs to be easily switched; therefore, it is often used to manufacture high-speed electronic devices.

High-performance optoelectronic devices have always been widely used in large-scale, flexible, transparent, high-speed, high-efficiency, broad-spectrum, low-power, and low-cost applications, and the unique optical properties of the 2D materials play a significant role in this direction. As a member of the 2D material family, the use of black phosphorus (BP) is widespread due to its extremely high hole mobility, good mechanical properties, and tunable energy band structure. The crystal structure of BP is shown in figure 3(b)-(i) [49], and the phosphorus atoms in the same layer are not on the same flat plane, indicating a honeycomb folded structure. The optical properties of the typical 2D materials (such as BP, TMDs, and Gr) are shown in figure 3(b)-(ii). The bandgap of BP can be adjusted from 0.3–1.5 eV by changing its thickness, which is just in the middle between the zero bandgap of Gr and the wider bandgap (1–2.5 eV) of TMDs. Under the external electric field, the Fermi level of the intrinsic monolayer Gr can be tuned to be 1 eV, covering the range from terahertz to visible light wavelengths.

Wang *et al* experimentally observed the unique piezoelectric effect in the 2D single-atom layer material of MoS<sub>2</sub> for the first time. Since then, research on the piezoelectric properties of 2D materials and related devices has been extensively focused. The essence of the piezoelectric effect is the displacement of ionic charges in the crystal (without a center of symmetry). When there is no strain, the distribution of charges on the lattice position is symmetrical, and the internal electric field is zero; when stress is applied to the crystal,



the charges are displaced. If the charge distribution is no longer symmetric, a net polarization will occur, accompanied by an electric field as a piezoelectric effect. As shown in figure 3(c)-(i), the lack of a symmetry center of the monolayer 2D h-BN is an important factor for its piezoelectricity [50]. Piezoelectric constants and coefficients ( $\epsilon_{11}$ ,  $d_{11}$ ) in 2D transition metal dichalcogenides (TMDCs) follow periodic trends, respectively (figure 3(c)-(ii)). The WS<sub>2</sub> has the smallest piezoelectric effect, and moving downward in group 6 (transition metals) or group 16 (chalcogenides) enhances the magnitude of the effect until MoTe<sub>2</sub>, with the largest coefficient, is reached. The 2D materials can withstand huge strains with high crystallinity, which are the research hotspots of high-performance piezoelectric materials [51–53]. Wu *et al* first proposed the piezoelectric performance of a single-layer MoS<sub>2</sub>-based device coupled with an external load resistor (figure 3(d)-(i)) [54]. After bending the device, the induced charge drives the flow of electrons in the external circuit, and when the substrate is released, the electrons flow in the opposite direction. Thus, the periodic bending and releasing enable the device to generate a piezoelectric output. Figure 3(d)-(ii) describes the piezoelectric signal's variation with increasing atomic layers (*n*). When  $n = 1, 3, 5$ , the piezoelectric response is significantly larger than that of  $n = 2, 4, 6$ , and is especially significant for the monolayer MoS<sub>2</sub>. The results indicate that the monolayer MoS<sub>2</sub> has a strong intrinsic piezoelectric response, and the periodic bending and releasing of the odd-numbered MoS<sub>2</sub> flakes produce a piezoelectric output. In contrast, the even-layered MoS<sub>2</sub> flakes have no outputs under bending strain, which is due to centrosymmetric bilayers, and the bulk crystals are non-piezoelectric.

Based on the above unique physical properties, adoption of 2D materials in tribotronic transistors will extensively extend and enrich this research field and inspire more innovations in sophisticated self-powered sensors, mechanical programming memory, interactive logic devices, and mechanoplastic artificial synapses.

### 3.2. Working mechanism in 2D tribotronic transistors

Understanding the triboelectric potential regulation process of traditional Si-based FETs is the basis for the research of tribotronic transistors. Zhang *et al* explored the working mechanism of Si-based FETs under TENG modulation [24]. The Al thin film serving as the transistor gate has a certain distance ( $d$ ) from the friction layer Kapton of the TENG device in the initial state (figure 4(a)-(i)). Under the action of external force, when the TENG is in contact with the Al of the FET gate, a negative electrostatic charge is left due to the stronger triboelectric negativity of the Kapton, and a positive electrostatic charge is retained on the Al layer (figure 4(a)-(ii)). In this state, Al is in full contact with the Kapton layer and results in an equilibrium state (no equivalent gate voltage applied to the transistor). When the external force is released, the Kapton film gradually separates from the Al, resulting in uneven distribution of triboelectric charges to form an electrostatic field (i.e. a triboelectric potential applied between the gate and source, figure 4(a)-(iii)). When the two friction layers of the TENG reach the maximum separation state, the triboelectric potential shows the maximum value (figure 4(a)-(iv)). Due to the extremely low resistivity of conventional Si substrates, the internal electric field is equivalently applied across the transistor as the gate voltage, and the energy band diagram is shown in figure 4(a)-(v). The charge polarization occurs in the top Si layer, attracting electrons and repelling holes to the bottom of Si. Since the main carriers in p-type Si are holes, this region forms a depletion region, which reduces the width of the conduction channel and thus reduces the output current. When the external force was applied to the TENG device again, the mobile layer of the Kapton gradually approached the Al film and, as the gate voltage decreased, the current flowed from the source electrode back to the mobile electrode (figure 4(a)-(v)). Therefore, via the contact and separation process of the two friction layers of the TENG, the internal gate voltage of the FET can be generated and controlled by an external force, which has the same effect as the applied gate voltage.

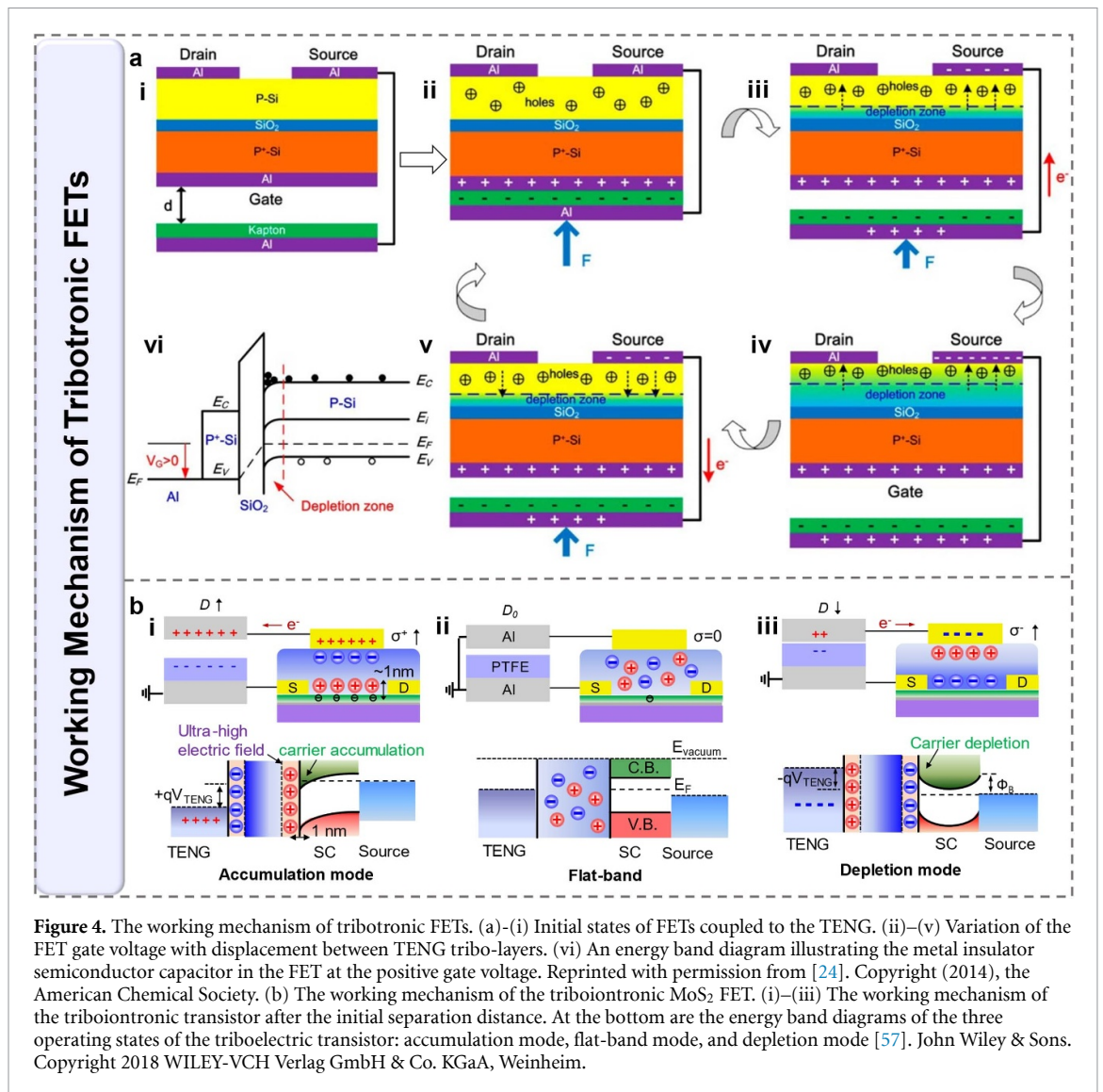
The reason for using the displacement stage to control the mechanical displacement of the TENG is to quantitatively explain that changing the distance between the friction layers in the TENG device produces different electric potentials. Therefore, the influence of the triboelectric potential generated by different TENG displacements on the performance of the device can be better analyzed. One of the friction layers of the TENG is used as a movable layer, while the other friction layer is usually set at the gate of the transistor device. When the displacement stage moves for a certain distance, the two friction layers contact each other. Due to the difference in electronegativity between the tribo-layers, the generated opposite charges will cause electrons to transfer, thereby forming a potential difference. The triboelectric potential generated in this process modulates the FET through the tribo-layer fixed on the gate of the 2D FET. Compared with the traditional gate voltage regulation of 2D FET, the regulation of the FET by the triboelectric potential generated by the contact and separation of the friction layers between TENGs can reduce the power consumption of the entire system to a certain extent. The role of the linear displacement stage is only to enable us to analyze the regulation ability of the FET accurately and quantitatively via different voltages generated by different displacements. Therefore, from the perspective of the whole system and architecture, using the triboelectric potential to control the FET can achieve low driving power and low system energy consumption.

The relationship between the internal positive gate voltage  $V_G$  applied through the TENG device and the distance  $d$  between the friction layers can be described by the following equation:

$$V_G = \frac{\varepsilon_K \cdot Q_0 \cdot d}{\varepsilon_0 \cdot \varepsilon_K \cdot S_0 + \varepsilon_0 \cdot C_{MIS} \cdot d_K + \varepsilon_K \cdot C_{MIS} \cdot d} \quad (1)$$

where  $Q_0$  is the amount of frictional surface charge,  $S_0$  is the frictional surface area, and  $\varepsilon_0$  and  $\varepsilon_K$  are the dielectric constants of vacuum and Kapton, respectively. Here,  $d_K$  is the thickness of the Kapton film, and  $C_{MIS}$  is the metal insulator semiconductor capacitance. However, the miniaturization process of traditional Si-based semiconductor devices is gradually approaching its physical limit, and there is still a development trend in this field to find new materials and develop new technologies to further reduce the size of devices. Traditional Si-based FETs require the channel thickness to be less than 1/3 of the channel length to effectively avoid short-channel effects. However, due to the limitations of traditional semiconductor materials, the thickness of the channel cannot be continuously reduced [55].

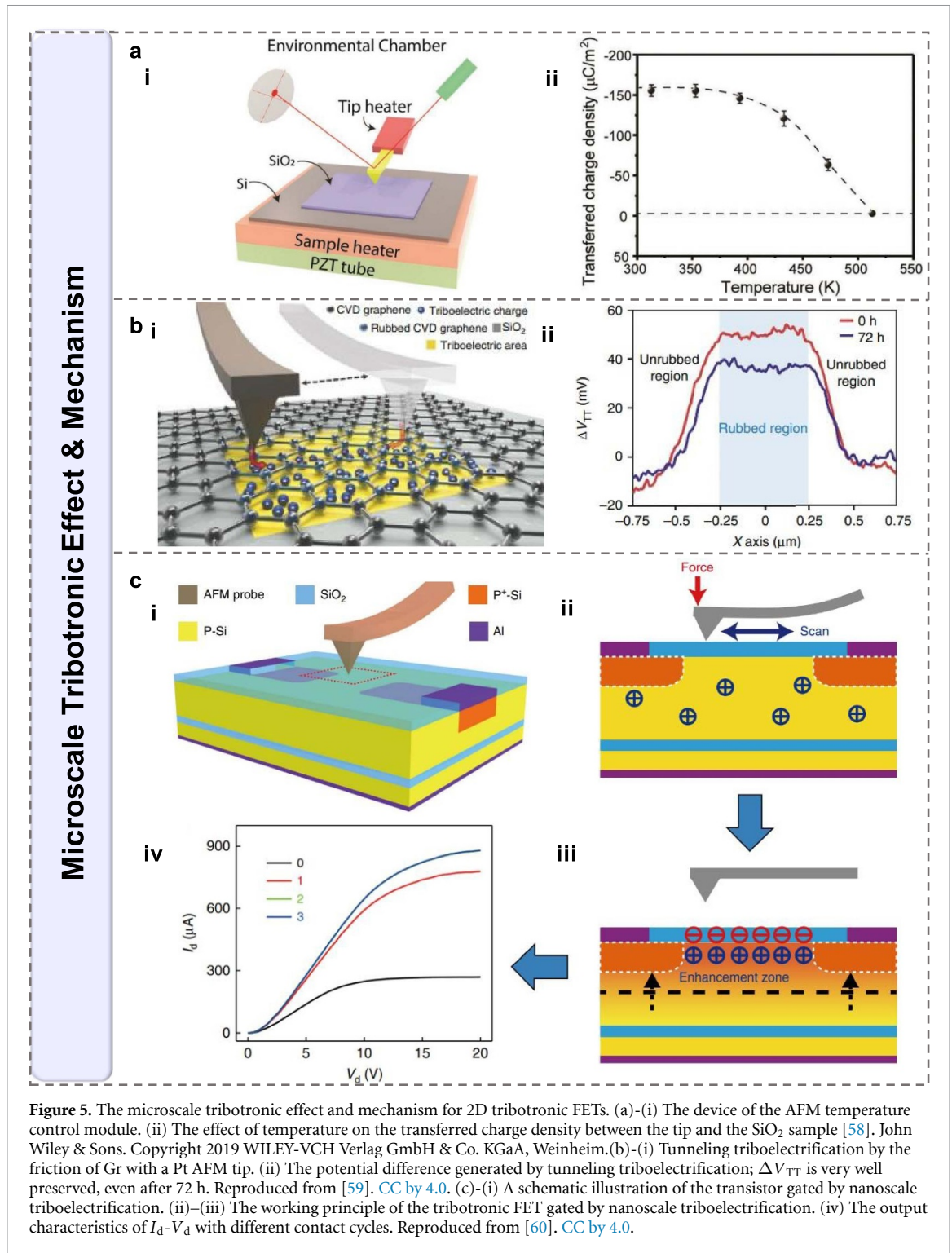
Those 2D materials with abundant valence band structures and readily controllable thicknesses exhibit great potential as next-generation channel materials [56]. Compared with traditional Si semiconductors, 2D semiconductors have enormous advantages in physical, electrical, and optical properties. Gao *et al* explored the regulation mechanism of the triboelectric potential in a 2D MoS<sub>2</sub> FET [57]. In the initial separated state



of the TENG in figure 4(b)-(ii), the induced charges are neutralized by grounding one of the electrodes or connecting the two electrodes. Therefore, no triboelectric potential is generated on the FET, showing a flat-band state, which has no effect on the Fermi level shift of MoS<sub>2</sub>. Among them, the triboelectric potential ( $V_{\text{TENG}}$ ) can be calculated using the following formula:

$$V_G = V_{\text{TENG}} = \frac{Q}{C_{\text{eff}}}. \quad (2)$$

When the displacement  $D$  is gradually increased (figure 3(b)-(i)), more positive charges are induced on the Al electrode and transferred to the gate, resulting in an equivalent positive gate voltage coupled to the MoS<sub>2</sub> channel. Under the ultra-high electric field, a high electron density is accumulated in the MoS<sub>2</sub> channel, which bends the energy band downward and lowers the energy barrier between the source and the MoS<sub>2</sub> channel. Therefore, it is easier for electrons to inject across the barrier into the conduction band, thereby increasing the output current. When the displacement  $D$  gradually decreases (figure 4(b)-(iii)), more positive charges are transferred from the gate to the Al electrode and neutralized with electrons in the polytetrafluoroethylene (PTFE). At the same time, the electrons are simultaneously transferred to the gate electrode, and the negative charge density ( $\sigma^-$ ) increases, resulting in a continuous increase in the negative gate charge (equivalent to an increase in the negative gate voltage). Therefore, in the flat-band state, the electrons remaining in the MoS<sub>2</sub> channel are effectively depleted, which bends the energy band upward and increases the energy barrier between the source electrode and the MoS<sub>2</sub> channel.



### 3.3. Microscale tribotronic effect and mechanism in 2D tribotronic FETs

It is significant to study the contact-electrification (or triboelectrification) mechanism in tribotronic FETs at the microscopic level, which is of great significance for exploring the origin of triboelectrification and implementing more precise mechanical friction control. The tribotronic FETs can be controlled by microscale friction using AFM or Kelvin probe force microscopy. As shown in figure 5(a)-(i), insulator materials (such as SiO<sub>2</sub>, Si<sub>3</sub>N<sub>4</sub>, Al<sub>2</sub>O<sub>3</sub>, and AlN) were chosen for the sample material deposited on a highly doped Si wafer with Au-coated Si tips as metal contact points [58]. The AFM tip heater and the sample heater are used to control the temperature of the tip and insulator material independently, and the entire temperature control module is placed in the Ar-filled airtight chamber. Correspondingly, the triboelectric charges are generated when the needle tip directly rubs against the sample surface for contact and separation. As shown in figure 5(a)-(ii), when the SiO<sub>2</sub> sample was in contact with the Au-coated tip, the density of the

transferred charges decreased with increasing temperature. When the temperature reached 513 K, the transferred triboelectric charges were completely eliminated, and the results were consistent with the electron thermionic emission theory during contact electrification. Electrons on the metal surface have sufficient kinetic energy of thermal motion to overcome the surface barrier. At low temperatures, the electron transfer and tunneling-back occur during the contact and separation process between the AFM tip and the sample surface. As the temperature increases, more electrons return to the metal tip through thermionic emission tunneling, and the results demonstrate that thermionic emission can influence the generation of triboelectric charges during contact electrification at the nanoscale.

Kim *et al* reported a tunneling triboelectrification method to localize electric charges transport in 2D materials, which was realized by using the AFM contact mode between chemical vapor deposition (CVD)-grown Gr (wet-transferred on SiO<sub>2</sub>/Si substrate) and an AFM tip coated with Pt (figure 5(b)-(i)) [59]. A portion of the triboelectric charge generated by the friction between the transferred Gr and the AFM tip passes through the Gr and is trapped at the interface. To characterize the obtained triboelectric potential of the Gr surface after rubbing with the AFM tip, the  $\Delta V_{TT}$  is defined as the net change in the surface potential due to the triboelectric tunneling charging in the rubbed region compared to the unrubbed region. Figure 5(b)-(ii) shows that the rubbed region of Gr is able to exhibit an effective electrostatic potential and exhibits good stability after 72 h. Bu *et al* analyzed the specific working principle of nanoscale triboelectric regulation on FET carrier transport based on the AFM contact mode to scan and rub the SiO<sub>2</sub> surface on top of the device for nanoscale triboelectrification [60]. As shown in figure 5(c)-(i), when the AFM probe touches the SiO<sub>2</sub> surface, a large number of charges are transferred to the SiO<sub>2</sub> surface (figure 5(c)-(ii)), generating an internal electric field in the channel region that attracts holes in the p<sup>+</sup>-Si layer and repels the electrons. Therefore, due to the increased hole concentration in the channel, an enhancement region is formed in the channel (figure 5(c)-(iii)). Figure 5(c)-(iv) indicates the output characteristic curves under different contact cycles of the AFM probe with the SiO<sub>2</sub> surface. As the number of contacts increases, more transferred charges are induced, and the drain current ( $I_D$ ) also increases. When the number of contact cycles is greater than two, the highest filled surface energy state of SiO<sub>2</sub> is almost as high as the Fermi level of the AFM Si probe due to the transferred charges, resulting in the drain current reaching saturation.

### 3.4. Macroscale tribotronic effect and mechanism in 2D tribotronic FETs

Using triboelectric potential regulation, the mechanism of the tribotronic effect on FETs is explored from a macroscopic point of view, which lays a theoretical foundation for practical applications of tribotronic transistors. Among different types of FETs, metal-oxide-semiconductor field effect transistors (MOSFETs) are typical electronic elements in integrated circuits due to their high input impedance, low drive power, and fast switching speed [61–64]. Peng *et al* theoretically investigated the triboelectric potential coupling (generated by contact electrification and electrostatic induction) to tune and control the charge carrier transport behavior in MOSFETs [34]. As shown in figure 6(a)-(i), the conventional tribotronic MOSFET consists of a conventional Si-based n-channel metal oxide semiconductor (NMOS) transistor, and the mobile triboelectrification layer consists of a PTFE film coated with an Al electrode. With the external mechanical displacements, the triboelectric charges with opposite polarities are generated during the contact and separation between the PTFE layer and the MOSFET. Electrostatic induction generates electric fields and potentials that result in a built-in voltage on the gate to tune and control the transporting properties between the drain and source. The two states of the moving electrode of the TENG in the grounding and floating states are defined as ‘short-circuit’ and ‘open-circuit’ states, respectively. The transport characteristics of the tribotronic NMOS are shown in figure 6(a)-(ii), with the dashed and solid curves representing the off and on states of the  $I_D$ , respectively. With the fixed  $V_D$ , the  $I_D$  in both states increases initially with a rapid increase and then becomes slower as the displacement of the TENG friction layer increases. With the increase in the  $V_D$ , the  $I_D$  exhibited a gradually increasing trend and the results showed that by adjusting the distance between the TENG triboelectric layer and the gate electrode, the FET could be effectively switched between the ‘on’ and ‘off’ states, acting as the fundamental theory for the research of tribotronic transistors.

To achieve a more efficient tribotronic tuned FET, Gao *et al* reported a 2D MoS<sub>2</sub>-based electric-double-layer (EDL) FET (i.e. triboiontronic transistors, figure 6(b)-(i)) [57]. The MoS<sub>2</sub> nanosheets were directly grown on Si/SiO<sub>2</sub> by CVD, and the source and drain electrodes were defined by electron beam lithography (EBL); the gate electrode was fabricated by thermal deposition. An encapsulation layer of PMMA is covered on the source and drain electrodes, and an ion-gel dielectric layer pattern is formed on the MoS<sub>2</sub> channel and part of the gate. The TENG device comprises a sandwich structure (Al/PTFE/Al) in contact-separation mode, which is connected in series to the side gate of the MoS<sub>2</sub> FET. According to the long-range polarization in ion-gel dielectrics, the triboelectric potential can be effectively coupled to the MoS<sub>2</sub> channel through the ultra-high capacitive EDLs. As shown in figure 6(b)-(ii), the equivalent gate-insulator-semiconductor (MIS) conduction mechanism is illustrated by the migration process of the

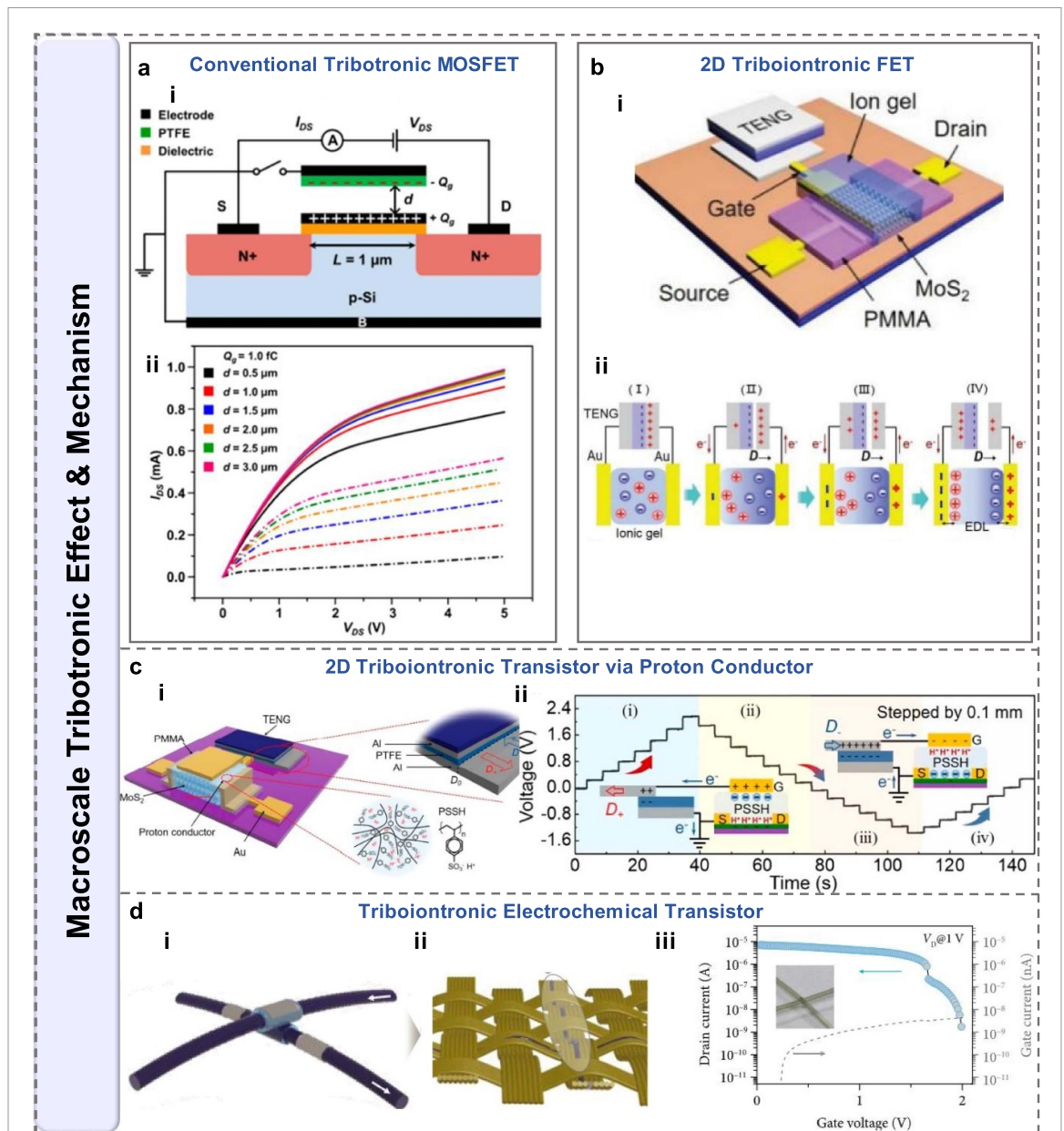


**Figure 6.** The macroscopic tribotronic effect and mechanism for 2D tribotronic FETs. (a)-(i) A schematic diagram of the device based on a TENG and a traditional Si-based n-channel MOSFET (NMOS). (ii) The  $I_D$ – $V_D$  output characteristics of triboelectric-potential-gated NMOS with  $Q_g$  of 1.0 fC under different  $d$  values from 0.5 to 3.0  $\mu\text{m}$ . Reprinted with permission from [34]. Copyright (2016), the American Chemical Society. (b)-(i) A schematic illustration of the tribotronic FET of  $\text{MoS}_2$ . (ii) Schematic illustrations of the generated TENG output voltage (equivalent to applied  $V_G$ ) under periodic displacement [57]. John Wiley & Sons. Copyright 2018, WILEY-VCH Verlag GmbH & Co. KGaA, Weinheim. (c)-(i) A schematic illustration of the tribotronic transistor via a proton conductor. Top inset: the enlarged structure of the TENG component. Bottom inset: the chemical structure of polystyrene sulfonic acid (PSSH). (ii) TENG output voltage (equivalent to the applied  $V_G$ ) according to periodic displacement. Reprinted with permission from [65]. Copyright (2020) the American Chemical Society. (d)-(i) A schematic diagram of a fiber-shaped tribotronic OECT that consists of a woven-structured TENG and a fiber-shaped OECT. (ii) The  $I_D$  and  $I_G$  in the logarithmic scale vs the  $V_G$  of the fiber-shaped OECT. From [38]. Reprinted from AAAS. CC BY 4.0.

ions in the metal/ion-gel/metal structure. When the two tribo-layers in the TENG are in the initial equilibrium state (I), no directional movement of charges occurs. However, when the two friction layers are separated by a certain distance (II), the induced charges are unbalanced, and directional movement occurs; therefore, the two electrodes are positively and negatively charged, respectively. More induced charges are transferred to the electrodes when the two tribo-layers are further separated (III–IV). As a result, the electrical field at the interface increases due to the triboelectric potential increasing.

A proton conductor is a specific ionic conducting material, via protons ( $\text{H}^+$ ), which has higher ionic conductivity due to the smallest size of protons, and is widely used in EDL transistors for low-voltage and high-frequency logic operations. This specific ionic material can also be used to extend the family of 2D tribotronic transistors. Yang *et al* reported a multifunctional tribotronic  $\text{MoS}_2$  FET via a proton

conductor (figure 6(c)-(i)) [65]. The MoS<sub>2</sub> was prepared using the mechanical exfoliation method and transferred to a SiO<sub>2</sub>/Si substrate, and a layer of PMMA was spin-coated on the source and drain electrodes. Then, standard proton conductor (polystyrene sulfonic acid, PSSH, its chemical structure is shown in the inset of figure 6(c)-(i)) was then spin-coated on PMMA as a dielectric layer. The sliding-mode TENG device is composed of the PTFE and Al friction layers, and the gating process is realized through proton conductors (figure 6(c)-(ii)). When a positive displacement (move toward outside) is applied to the TENG (a), the output voltage gradually increases from 0 to 2.15 V and partial induced charges are transferred to the gate. When a negative displacement (move toward inside) at the same distance is applied to the TENG, the output voltage gradually recovers to 0 V (b). When the TENG sliding displacement is further reduced to  $-0.7$  mm (c), the output voltage drops to  $-1.36$  V due to the positive triboelectric charges confined to the TENG contact surface; when the sliding displacement gradually returns to the initial position, the output voltage gradually returns to the initial position of 0 V. Therefore, the device can utilize the triboelectric potential generated by mechanical displacement to tune the electrical properties of FETs through proton migration.

The electrochemical transistor is the other type of ion-controlled transistor, which widely uses conductive polymer poly(3,4-ethylenedioxythiophene)/poly(styrene sulfonic acid) (PEDOT:PSS) as the channel due to its high conductivity and good processing properties. Recently, researchers have discovered that applying a triboelectric potential to modulate the doping state in conducting polymers can achieve an efficient combination of mechanical action and electrochemical reactions in OECTs. For instance, Yu *et al* reported a fiber-shaped tribotronic electrochemical transistor comprising a fiber-shaped PEDOT:PSS OECT and a woven contact-separation-mode TENG cloth (figure 6(d)) [38], which has been used for motion sensor and logic devices. To achieve effective triboelectric potential gating and diminish the leakage current, the nylon fibers with the surface-dip-coated PEDOT:PSS channel layer were first cast with 70 wt% ion-gel and then cast with 90 wt% ion-gel to improve the gating efficiency.

## 4. Applications of 2D tribotronic transistors

The 2D tribotronic transistor is a new type of electronic device that has developed rapidly in recent years that utilizes a TENG triboelectric potential instead of a traditional gate voltage to control the transistor device. The drain–source current can be directly controlled by external mechanical behavior. Therefore, 2D tribotronic transistors have a larger sensing range to the external environment. And the active materials can be extended to common semiconductors and other materials used for contact electrification [66], promising broad application prospects in sensing, flexible electronics, human–machine interfaces, etc. This section mainly summarizes applications based on 2D tribotronic transistors in different fields, such as smart sensors, logic devices, memory devices, and artificial synapses. Table 2 shows the friction materials, 2D channel materials, and output performance of 2D tribotronic transistors according to different applications. Appropriate TENG friction materials and 2D channel materials can be selected according to the target applications.

### 4.1. Intelligent sensors based on 2D tribotronic FETs

At present, the world has entered the era of intelligence, and sensors have become a general technology. Improvement of the sensor industry directly determines the degree of intelligent development [27, 73–75]. With the rapid development of self-powered sensors and systems, the TENG itself has already been successfully applied in different types of sensors (e.g. flexible sensors [76], pressure sensors [77], biological sensors [78]) and has made significant contributions and achievements in the Human Machine Interface [79, 80]. In contrast, a 2D tribotronic transistor is a device that regulates the electrical transport capability of a semiconductor through an electric field, and intelligent sensors are one of the important directions of its functional application research. The 2D tribotronic transistor combines FET devices with special identification elements compared to the use of conventional TENG applications as sensors. The application of a gate voltage can induce carriers at the interface of the insulating layer to form a conductive channel, and the carriers are injected from the source and efficiently transported from the conductive channel to the drain driven by the source–drain voltage. Therefore, an FET mainly includes two basic physical processes: carrier injection and carrier transport. The working principle of the 2D tribotronic-transistor-based sensor is that the detected object affects the electrical signal of the 2D tribotronic transistor by changing the injection and transmission characteristics of carriers, thereby realizing the sensing function via quantitative signal conversion. It is worth noting that, due to the regulation characteristics of the TENG triboelectric potential instead of the traditional gate voltage, the sensor also has the function of signal amplification. Therefore, sensors based on 2D tribotronic transistors can theoretically exhibit higher sensing sensitivity.

Human tactile sense is one of the most common forms of perception, second only to vision, that is used to obtain environmental information, and it is a necessary medium to interact with the environment directly.

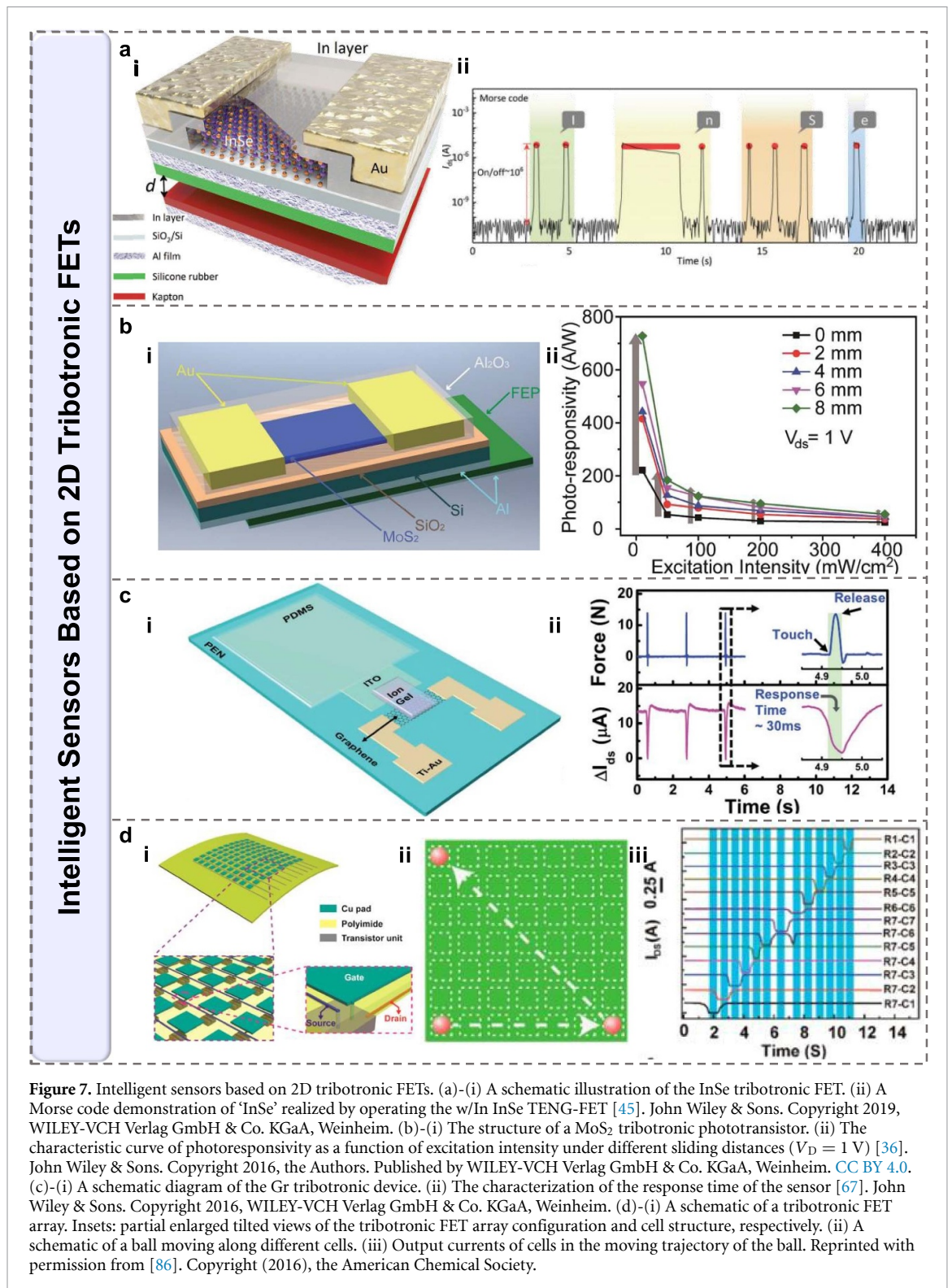
**Table 2.** A comparison of 2D tribotronic transistors and their output performance based on different applications.

References	Applications	Friction Layers	2D Materials	ON/OFF Ratio
[45]	Intelligent sensors	Silicone rubber/Kapton	InSe	$10^6$
[36]	Intelligent sensors	Al/FEP	MoS <sub>2</sub>	$10^3$
[67]	Intelligent sensors	polydimethylsiloxane (PDMS)/object	Gr	2.96
[43]	Intelligent sensors	PDMS/PMMA	Gr	3
[44]	Intelligent sensors	PTFE/Al	MoS <sub>2</sub>	$10^3$
[37]	Logic devices	PTFE/Al	MoS <sub>2</sub> /BP	$1.1 \times 10^6$
[46]	Memory devices	PTFE/Cu	Gr/h-BN/MoS <sub>2</sub>	$10^5$
[68]	Memory devices	Al/PTFE	MoS <sub>2</sub>	$10^7$
[69]	Memory devices	External touch/PDMS	MoS <sub>2</sub>	$10^5$
[70]	Artificial synapses	Kapton/silicone rubber	InSe/h-BN/Gr	$10^4$
[71]	Artificial synapses	Cu/FEP	Gr/h-BN/WSe <sub>2</sub>	$10^6$
[72]	Artificial synapses	Cu/FEP	MoS <sub>2</sub>	$10^5$
[40]	Artificial synapses	PTFE/Cu	Gr/MoS <sub>2</sub>	1.53
[29]	Artificial synapses	PTFE/Cu	Gr	2.43

The tactile sense shows a strong sensitivity and can directly help to recognize various properties of objects and the environment, which is considered an intelligent connector between sensation and action. From this perspective, research on tactile sensors is non-negligible [47, 81]. Li *et al* reported a 2D In-doped InSe-based tribotronic FET (figure 7(a)-(i)) that was effectively applied in tactile sensors [45]. The triboelectric potential generated by the TENG can be used as the gate voltage to adjust the carrier transport behavior in the electronic device, in which the TENG unit is composed of two tribo-layers of Kapton and silicone rubber. Several layers of the InSe flakes were obtained by mechanical exfoliation of InSe bulk crystals grown via chemical vapor transport and then deposited on the SiO<sub>2</sub>/Si substrates, and a 32 nm thick In layer was deposited on top of the InSe flakes to enhance the carrier injection and device stability. An Al electrode layer is deposited on the bottom of the SiO<sub>2</sub>/Si substrate to ensure ohmic contact before coupling with the TENG. Simultaneously, it acts as a TENG electrode, and a silicone rubber layer is attached to it as a triboelectrically charged layer. Another layer of Al is attached to the bottom of the moving Kapton layer, which is used as another triboelectrically charged layer. The two layers of Al are used as the charge-inducing material. The sensitivity of the triboelectric switches determines its potential applications in tactile sensors and functional electronics. Using finger-touch control, the instantaneous switching and holding of the on/off state of the InSe FET can be effectively achieved (figure 7(a)-(ii)). The simple operation illustrates the practical properties of tribotronic transistors as integrated tactile sensors or tactile switches.

With the development of phototransistors, the traditional method of applying a high gate bias voltage to increase the photocurrent brings with it additional energy consumption. Researchers found that the triboelectric regulation of the TENG can significantly improve the photoelectric response of the FETs, providing a method for the research of the tribotronic transistor in the field of photoelectric sensors [82–84]. As a Gr-like monolayer transition metal compound, MoS<sub>2</sub> is one of the materials with the best optoelectronic properties among all the available 2D semiconductor materials. Due to its excellent optical and electrical properties, the single-layer structure has great prospects for assisting or replacing Gr. The MoS<sub>2</sub> with a thickness of one atomic layer is a 2D direct bandgap semiconductor material, which can be used to develop advanced nano-electronic and functional optoelectronic devices. Pang *et al* reported a novel tribotronic phototransistor composed of a MoS<sub>2</sub> FET and a sliding-mode TENG (figure 7(b)-(i)) [36]. Based on simple mechanical exfoliation, a few layers of the MoS<sub>2</sub> were fabricated on a p-type Si substrate, and the source and drain electrodes were prepared by ultraviolet (UV) lithography and electron beam evaporation; moreover, an Al film was deposited on the Si substrate as a gate. The TENG device consists of an inductively coupled plasma etched fluoroethylene propylene (FEP) film and a 50 μm thick Al foil. Under different sliding distances, the photosensitization characteristics of the device under different photoexcitation intensities are shown in figure 7(b)-(ii). At a drain voltage of 1 V and light intensity of 10 mW cm<sup>-2</sup>, the photoresponsivity is significantly enhanced as the relative sliding distance between the bottom TENG tribo-layer and the device increases. Therefore, changing the sliding distance can effectively and stably adjust the photocurrent. Due to the saturation of trap states at the interface of MoS<sub>2</sub> and the substrate, the photoresponsivity and the triboelectric charging enhancement value tend to decrease with the increase in the photoexcitation intensity.

The excellent electrical conductivity and light transmittance also make Gr able to be used as a transparent conductive electrode material, which demonstrates outstanding applications in touch screens, liquid crystal displays, etc [85]. Therefore, Gr is considered the most potential replacement for indium tin oxide (ITO) in touch screen manufacturing. Khan *et al* reported a Gr tribotronic FET for electronic skin and touchscreen



applications [67]. The ITO electrode and PDMS tribo-layer combined with the TENG device, Gr channel, and ITO electrode are coupled in a coplanar manner through 1-ethyl-3-methylimidazolium bis(trifluoromethyl sulfonyl) imide-based ([EMIM][TFSI]) ion-gel gate dielectrics (figure 7(c)-(i)). The triboelectric potentials generated by device contact with external objects are used as the gate bias to tune current transport in the Gr FETs. Figure 7(c)-(ii) demonstrates the sensor response characteristics based on the Gr tribotronic FET. Using an Al sheet as the touch object, a commercial triboelectric force sensor was used to measure the applied force, and its response was used as a reference value. The sensor responds rapidly to the touch stimuli with a response time of about 30 ms (time from touch to the peak) with very high sensitivity. Furthermore, the Gr tribotronic sensor array can spatially map various touch stimuli, such

as multi-touch stimuli and the trajectory of a moving ball, which is of great significance for electronic skin applications.

Due to the popularization of intelligent products, electronic devices show considerable market prospects. As one of the key core components, sensors will affect the devices' functional design and future development [86–90]. Yang *et al* reported a sensor based on a tribotronic transistor array, which can realize trajectory tracking recognition and motion monitoring through tactile contact (figure 7(d)-(i)) [91]. Each element of the sensor array consists of a TENG and an FET. The PTFE film and the Cu sheet constitute the TENG, and the gate of the FET is connected to the Cu sheet by a hole. The motion paths of the ball in the sensor array (figure 7(d)-(ii)) are in good agreement with the signal changes, as shown in figure 7(d)-(iii). Two current drops were observed in the  $I_D$  response of R7-C6, and the second current drop could be explained by turning the moving ball in a diagonal direction. Experiments have verified that the tribotronic FET has real-time tracking capability and good practicability in dynamic motion monitoring and trajectory tracking.

#### 4.2. Logic devices based on 2D tribotronic transistors

The generation of too much heat during operation, poor reliability, slow computing speed, high price, and large size are the drawbacks of electronic tube components that have limited the development of the first version of computers. Since the invention of the FET, electronics have made a real leap in progress. FETs began to be used as components in second-generation computers. In the process of regulating a 2D tribotronic transistor, four different working modes of a TENG can be selected according to desired applications, including vertical contact-separation mode, lateral sliding mode, single-electrode mode, and freestanding triboelectric-layer mode. For the TENG in vertical contact-separation mode [92], when two dielectric films of different materials are in contact with each other, surface charges with opposite signs are formed on the two contact surfaces. When the two surfaces are separated due to an external force, an induced potential difference is formed between the back electrodes of the two friction layer materials. In addition, triboelectric charges (horizontal sliding mode) are generated on the two surfaces when there is relative displacement between the two friction materials [93]. Therefore, polarization is formed in the horizontal direction, driving electrons to flow between the upper and lower electrodes to balance the electrostatic field generated by the triboelectric charge. Unlike the previous two modes that use two electrodes, the single-electrode mode has only one electrode, which is better suited for complex electrical connections [94]. The charged object at the free end approaches or leaves the material connected to the gate, which will change the local electric field distribution and cause a change in potential. If the backside of the friction layer is plated with two disjointed symmetrical electrodes, the reciprocating motion of the charged object between the two electrodes will create a potential difference between the two electrodes, which causes electrons to flow back and forth between the two electrodes (freestanding triboelectric-layer mode) [95]. Therefore, researchers can choose different working modes of the TENG according to specific application scenarios to achieve the desired results. Different working modes are essentially mechanical displacement modulation, and a linear displacement stage can be used to quantitatively analyze the ground potential differences of different magnitudes generated under different displacements.

According to the FET's performance, an FET-based logic circuit can be realized and is widely used in digital integrated circuits [25, 39, 96–100]. Zhang *et al* reported a floating-gate tribotronic FET based on a triboelectric layer and conventional Si-based FETs [101]. A Si metal oxide FET with a floating-gate electrode is integrated into the FR4 layer, and a Cu film is sputtered onto the upper side of the FR4 layer connected to the floating-gate electrode via holes. The two Cu electrodes deposited on the backside of the n-type channel layer act as the bottom drain and source, and the Cu film on the upper side of the FR4 layer is used as one of the friction layers of the TENG device, with the other friction layer consisting of a movable FEP film. The triboelectric charges generated between the tribo-layers can modulate the charge carrier transport in the FETs. By integrating a tribotronic FET and a conventional p-type MOSFET on the lower FR4 layer and another tribotronic FET and a conventional n-type MOSFET on the upper FR4 layer, a NAND logic circuit can be formed (figure 8(a)-(i)). A schematic diagram of the device-based tribotronic NAND gate is shown in figure 8(a)-(ii). For an instant, when the input state (EA, FB) is (0, 0) and the input EA is 0 V, the FEP layer is in full contact with a Cu friction layer ( $d = D_0$ ). The top half is 'on' and the bottom half is 'off'. Therefore, the output voltage is  $5.033 \pm 0.021$  V, corresponding to a logic '1'. Accordingly, the NAND gate logic circuit of EA and FB can be realized by controlling the contact distance between the input voltage and the friction layer. Moreover, the basic units of logic circuits such as S-R flip-flop, D flip-flop, and T flip-flop, are realized by further assembling the tribotronic NAND gate and traditional digital circuit.

Moore's law states that the number of FETs that can be accommodated on an integrated circuit doubles approximately every 18–24 months. However, as the traditional FETs shrink in size, the short-channel effect becomes more pronounced, where the gate electric field cannot perform the full effect, resulting in leakage currents that affect the performance of the FET. To address these issues, FETs based on 2D materials have

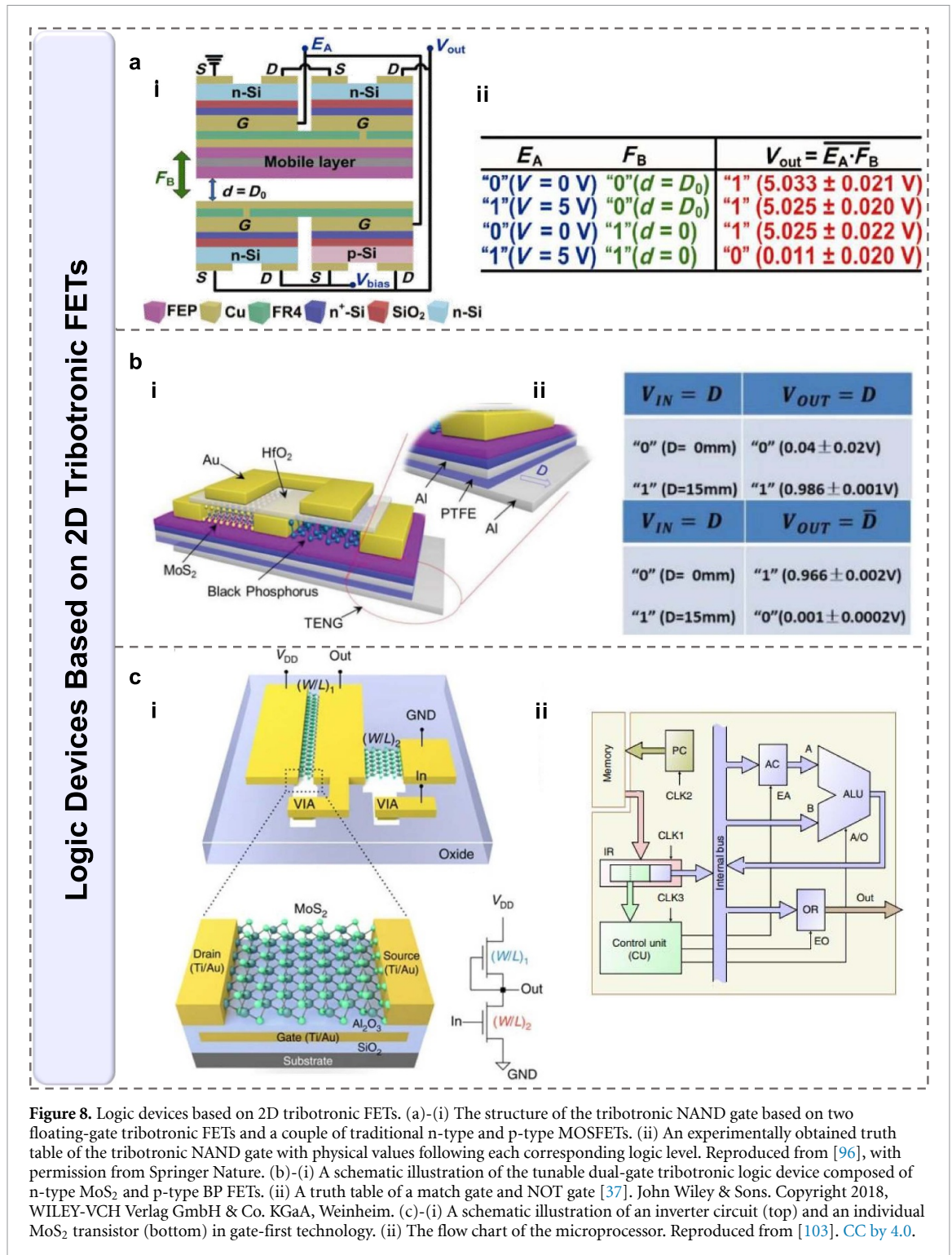


**Figure 8.** Logic devices based on 2D tribotronic FETs. (a)-(i) The structure of the tribotronic NAND gate based on two floating-gate tribotronic FETs and a couple of traditional n-type and p-type MOSFETs. (ii) An experimentally obtained truth table of the tribotronic NAND gate with physical values following each corresponding logic level. Reproduced from [96], with permission from Springer Nature. (b)-(i) A schematic illustration of the tunable dual-gate tribotronic logic device composed of n-type MoS<sub>2</sub> and p-type BP FETs. (ii) A truth table of a match gate and NOT gate [37]. John Wiley & Sons. Copyright 2018, WILEY-VCH Verlag GmbH & Co. KGaA, Weinheim. (c)-(i) A schematic illustration of an inverter circuit (top) and an individual MoS<sub>2</sub> transistor (bottom) in gate-first technology. (ii) The flow chart of the microprocessor. Reproduced from [103]. CC by 4.0.

been extensively studied because of their ability to reduce the short-channel effects due to the atomic thickness [66, 102–104]. In addition, the coupling between the triboelectric potential and electrical behavior in semiconductor materials enables the unprecedented device properties [105–107]. Gao *et al* reported a tunable tribotronic dual-gate logic device based on the n-type MoS<sub>2</sub> FET, p-type BP FET, and a sliding-mode TENG (figure 8(b)-(i)) [37]. The triboelectric potential generated by the TENG can effectively drive the FETs and logic devices without a gate voltage. Using SiO<sub>2</sub> as the bottom gate dielectric layer, the MoS<sub>2</sub> nanosheets were grown on the SiO<sub>2</sub>/Si substrate via the CVD method. Meanwhile, the Cr/Au source–drain electrodes were determined by standard EBL and electron beam deposition. HfO<sub>2</sub> grown via atomic layer deposition (ALD) was applied as the top-gate dielectric layer for efficient modulation of the carrier transport in the FET channel, followed by top-gate electrode deposition by EBL and metallization. PTFE was used as one of the

friction layers in the TENG device, and the other friction layer was an Al tape attached to a moving acrylic plate. During the TENG device sliding process, the triboelectric potential can be generated by triboelectric charging and electrostatic induction and is used as a voltage input through the bottom gate. Figure 8(b)-(ii) demonstrates the truth table corresponding to the device logic states with the TENG sliding distance. It is defined that the initial position ( $D = 0$  mm) of the TENGs is the '0' state, and the separation position ( $D = 15$  mm) is the '1' state. When the MoS<sub>2</sub> FET is grounded, the output voltage of the tribotronic logic inversion changes from a low level ( $V_{\text{OUT}} = 0$ ) to a high level ( $V_{\text{OUT}} = 1$  V), and the TENG changes from the '0' state to the '1' state. When the BP FET is grounded, the output voltage of the triboelectric logic inverter changes from a high level ( $V_{\text{OUT}} = 1$  V) to a low level ( $V_{\text{OUT}} = 0$ ), and the TENG changes from the '0' state to the '1' state.

With the rapid development of electronic computers and digital information, there is an increasing demand for the number of FETs in integrated circuits. The logic calculation of a single FET cannot meet the computer processing requirements, and some researchers have devoted themselves to the study of multiple cascading FETs for the logic calculation. Wachter *et al* reported a 2D MoS<sub>2</sub> FET-based microprocessor (figure 8(c)-(i)) that can achieve the computational power of cascaded logic [108]. The bottom metal (gate) layer was patterned by EBL and Ti/Au evaporation, and then the Al<sub>2</sub>O<sub>3</sub> gate oxide was deposited using ALD. The FET channel was fabricated using large-area bilayer MoS<sub>2</sub> films grown via CVD. After transferring the MoS<sub>2</sub> films to the target wafers, 18 FET devices were fabricated per wafer substrate. Figure 8(c)-(ii) is the flow chart of the microprocessor, and the arithmetic logic unit (ALU) forms the core of the entire processor. The experiments, together with a series of logic analysis operations, further demonstrate the capability of 2D semiconductor-based cascaded logic. The reported 2D MoS<sub>2</sub> FET-based device performs complex logic calculations on the entire microprocessor. This kind of microprocess also exhibits great potential to be integrated with TENG components to achieve the mechanical-behavior-controlled counterparts.

#### 4.3. Memory devices based on 2D tribotronic transistors

Since the appearance of FETs, the prosperity of electronic products has been achieved. Therefore, the FET is also known as the greatest invention of the 20th century [109–112]. Its appearance laid the foundation for the generation of integrated circuits, microprocessors, and computer memory. A latch structure made of FETs can store the states of '0' or '1'. The FET is made into a floating-gate structure, with the amount of charge stored in the gate affecting the threshold voltage of the FET, and the information in the memory can be read out through the difference in the threshold voltage. Accordingly, FETs play a necessary role in memory devices to process massive amounts of data in the era of the IoTs [113–116]; however, the storage state in traditional storage devices is limited by electrical or optical signals.

The pioneering field of tribotronics was first proposed in 2014 by coupling triboelectric potential with semiconductors. The TENG component integrated in the 2D tribotronic transistor can control the 2D FET by controlling the signal generated by external mechanical displacement instead of the traditional gate voltage [117]. In contrast to traditional regulation using gate voltage, TENG devices do not require an additional power supply, and only use friction between different materials to drive electrons and generate the corresponding triboelectric potential. In the process of friction regulation, a small displacement between the TENG friction layer materials can make the whole device achieve a fast response, which provides a path for the development of highly sensitive tribotronic devices. Since the contact and separation between the friction materials avoid direct contact with the electrodes, the durability and the degree of wear resistance are also improved to a certain extent. In addition, the TENG has been confirmed to have greater durability when interacting with the external environment [118], laying an important foundation for the development of tribotronics. FETs based on mechanical tribotronic control have the characteristics of low power consumption, high sensitivity, and strong stability, and have emerged as an efficient mechano-memory in recent years. Jia *et al* reported a novel multi-bit tribotronic non-volatile memory based on a Gr/h-BN/MoS<sub>2</sub> heterostructure and a TENG [46]. As shown in figure 9(a)-(i), the MoS<sub>2</sub> flakes on top act as conductive channels with the Gr on the SiO<sub>2</sub>/Si substrate serving as a floating-gate electrode, and the h-BN flakes sandwiched between them serve as a suitable tunneling barrier. The materials of the two friction layers of the TENG device are the PTFE film and Cu on the back of the Si wafer, respectively. When the two tribo-layer materials experience periodic contact-separation, the triboelectric charges can be induced and coupled to the FET through the bottom gate. Varying the contact-separation distance between the two friction layers of the TENG can provide different voltages to motivate the memory device efficiently. The memory is first programmed by mechanical displacement for 1 s. As the separation distance gradually increases (0.05 mm per step), the corresponding triboelectric potential pulse can gradually attract more and more electrons into the Gr layer and increase the current (figure 9(a)-(ii)). Therefore, the tiny adjustment between the friction layers can successfully realize the dynamic modulation of charge carrier storage. The working principle of the

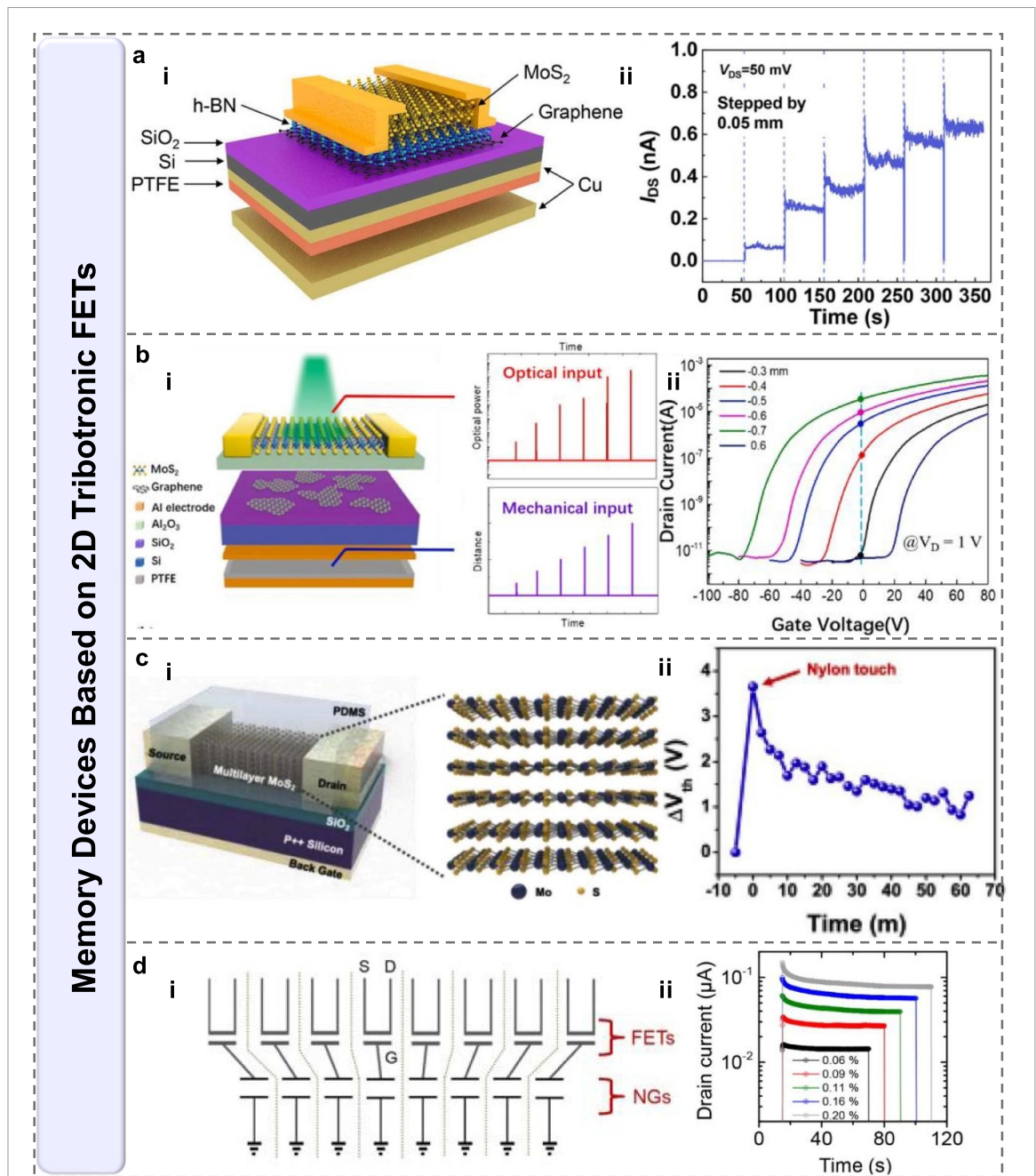


**Figure 9.** Memory devices based on 2D tribotronic FETs. (a)-(i) A schematic diagram of the memory device based on a Gr/h-BN/MoS<sub>2</sub> heterostructure floating-gate FET and a TENG device. (ii) The curve of  $I_D$  versus time when the friction layer distance is 0.05 mm. Reprinted from [46]. Copyright (2021), with permission from Elsevier. (b)-(i) A schematic illustration of the MoS<sub>2</sub> electromechanical and photoelectronic memory device structure with the NG as the charge trapping layer. (ii) The transfer characteristics of the MoS<sub>2</sub>-based memory device under different TENG movements. Reprinted from [68]. Copyright (2021), with permission from Elsevier. (c)-(i) A schematic illustration of the MoS<sub>2</sub> tribotronic touch memory device structure. (ii) Time evolution of the threshold voltage shift,  $\Delta V_{th}$ , due to the nylon touch. Reprinted from [69]. Copyright (2020), with permission from Elsevier. (d)-(i) A circuit diagram of the memory array. (ii) The current characteristics of the piezopotential-programmed non-volatile memory under various bending strains. Reprinted with permission from [114]. Copyright (2016), the American Chemical Society.

triboelectric potential on non-volatile memory is similar to applying a gate voltage, which ensures that the triboelectric-regulated FET memory possesses good stability and reliability.

Due to the requirements for device miniaturization, multilevel memory has remarkable development potential in the semiconductor industry. Zhao *et al* reported a 2D FET-based mechanoplastic triboelectric memory (figure 9(b)-(i)) [68]. The nano-Gr was directly grown on a heavy phosphorus-doped Si substrate with SiO<sub>2</sub> by plasma-enhanced CVD. A 10 nm Al<sub>2</sub>O<sub>3</sub> deposit via ALD is used as a tunneling dielectric layer, and Ti/Au is used as the source–drain electrode. A sandwich-structured Al-PTFE-Al-based TENG device was connected to the FET back gate to convert the mechanical signals to electrical signals. The triboelectric potential generated by the mechanical motion between the TENG tribo-layers can transfer the electrons

between the MoS<sub>2</sub> and the NG floating gate, resulting in a charge trapping/releasing process. The right inset of figure 9(b)-(i) shows the optical and mechanical outputs of the mechanoplastic tribotronic FET, and the TENG tribo-mechanically regulated FET storage characteristics are shown in figure 9(b)-(ii). When an appropriate mechanical pulse (positive output voltage generated by the forward motion of the TENG) is applied to the device, the electrons can tunnel from MoS<sub>2</sub> to the nano-Gr layer due to the lowered tunneling barrier, enabling the erasing process. Conversely, the negative output voltage generated by the reverse motion of the TENG prompts the electrons trapped in the nano-Gr layer to tunnel back to the MoS<sub>2</sub> channel, leading to the programming process. The distance between the TENG friction layers was  $-0.3$  to  $-0.7$  mm for the programming process and returned to  $0.6$  mm for data erasing. The program/erase current ratio can reach  $10^7$  to provide a stable and distinguishable multilevel memory state.

With the rapid development of electronic devices, zero power consumption during memory writing has become a research hotspot. Khan *et al* reported a tribotronic MoS<sub>2</sub> touch memory with zero power for the writing process [69]. Figure 9(c)-(i) indicates the 2D MoS<sub>2</sub>-based triboelectric memory structure and the atomic structure of MoS<sub>2</sub> (right). The  $20\ \mu\text{m}$  thick PDMS receives external touch stimuli and protects the underlying extremely thin MoS<sub>2</sub> channel from any possible direct contact destructiveness. To characterize the tactile memory properties of the device, positively charged nylon was rubbed against the PDMS surface to induce negative charges due to the triboelectrification effect. As shown in figure 9(c)-(ii), when a touch operation is performed, the threshold voltage of the device increases to a peak value of about  $3.5$  V. As the charge on the PDMS is well maintained, the threshold voltage decays slowly and the triboelectric charges generated on the PDMS surface after touch act as a gate bias to control the electron transport in the underlying 2D MoS<sub>2</sub> channels. Notably, during the writing process, no power is consumed. Moreover, simple touch action through a conventional p++ Si bottom gate can change the output current by more than two orders of magnitude during the reading process.

A single FET is far from meeting the demands of memory development in the future, and the cascade of multiple FETs and NG integrated devices can realize multilevel data storage. Sun *et al* reported a mechanical strain triggered array-type multilevel memory [119]. Figure 9(d)-(i) indicates the equivalent circuit diagram of the memory device array. A single device consists of one ion-gel FET coupled with one NG. The IGZO and polyvinylidene fluoride-trifluoroethylene (PVDF-TrFE) materials are used as the channel layers and energy-supplying layers, respectively. The electrostatic potential generated by the NG under external strain replaces the conventional gate voltage for the program/erase operation of the memory, therefore, reducing the power consumption. The electrostatic potential can maintain the induced charge in the FET channel, even after the strain is released. As shown in figure 9(d)-(ii), after disconnecting the top electrode of the NG from the ground, the continuous and stable leakage current indicates the possibility of an electrostatic potential-driven FET as a memory device. After the strain is applied, the connection to the ground is cut to realize the programming process for storing the data. Erasing the memory is achieved by reconnecting the top electrode of the NG to the ground. Under strain conditions, the array device can achieve 2-bit multilevel data storage (more than four levels), showing ideal memory performance. Simultaneously, the induced electrostatic potential under external strain replaces the traditional gate voltage input, effectively reducing power consumption.

#### 4.4. Artificial synapses based on 2D tribotronic FETs

The essence of synaptic plasticity is the ability of a synapse to strengthen or weaken over time in response to an increase or decrease in activity [120–122]. As the memory is hypothesized to be represented by the extensively interconnected neural circuits, synaptic plasticity is considered one of the important neurochemical underpinnings of learning and memory. Gao *et al* reported contact-electrification-modulated heterostructure FETs for synapse simulation [70]. Figure 10(a)-(i) demonstrates the information transmission mechanism at the biological synapses in neurons. When the tactile signals stimulate the synapses through the central nervous system, the presynaptic membrane will release neurotransmitters to the synaptic cleft and interact with the receptors in the postsynaptic membrane to induce an excitatory or inhibitory postsynaptic potential [123]. Therefore, the excitatory postsynaptic current (EPSC) or inhibitory postsynaptic current (IPSC) generated during the inner-synaptic information transmission is a vital indicator for evaluating the strength of synaptic connections. The device consists of a 2D InSe floating-gate FET and a TENG device (figure 10(a)-(ii)). The FETs with InSe/h-BN/Gr heterostructures were fabricated on heavily doped Si substrates with SiO<sub>2</sub> layers. The TENG is located under the Si layer and consists of an Al film, a Kapton layer, a silicone rubber layer, and an Al film from bottom to top. Based on the triboelectric synaptic devices, the injection/release of pulse-induced charges in the touch-modulated Gr floating gate (as charge storage layers) resembles the touch-controlled neurotransmitter influx process in synapses. The Kapton and silicone rubber layers are the two friction layers of the TENG, and the input signal obtained by adjusting the distance between them can induce the output current as a postsynaptic current (PSC). The

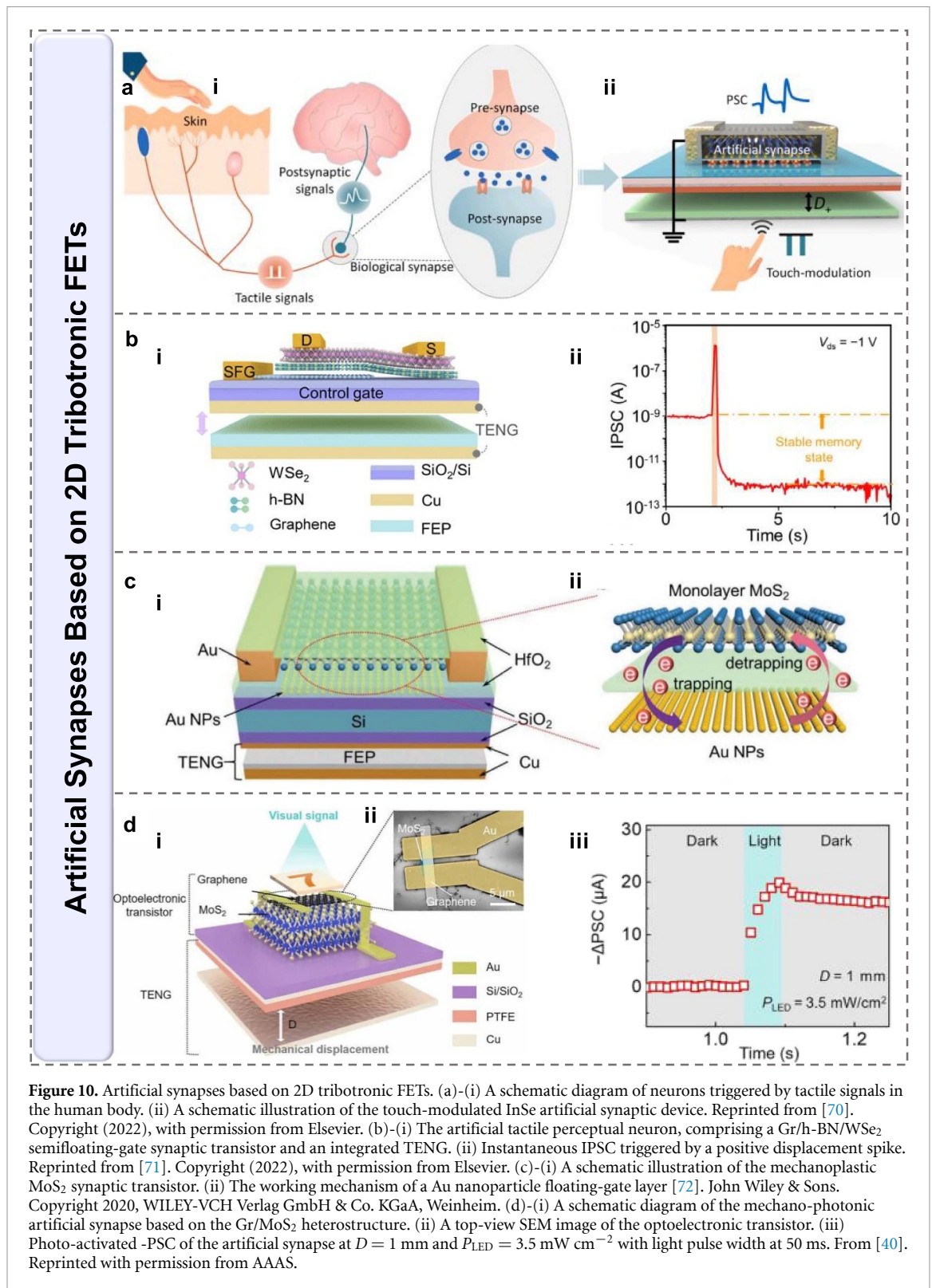


**Figure 10.** Artificial synapses based on 2D tribotronic FETs. (a)-(i) A schematic diagram of neurons triggered by tactile signals in the human body. (ii) A schematic illustration of the touch-modulated InSe artificial synaptic device. Reprinted from [70]. Copyright (2022), with permission from Elsevier. (b)-(i) The artificial tactile perceptual neuron, comprising a Gr/h-BN/WSe<sub>2</sub> semifloating-gate synaptic transistor and an integrated TENG. (ii) Instantaneous IPSC triggered by a positive displacement spike. Reprinted from [71]. Copyright (2022), with permission from Elsevier. (c)-(i) A schematic illustration of the mechanoplastic MoS<sub>2</sub> synaptic transistor. (ii) The working mechanism of a Au nanoparticle floating-gate layer [72]. John Wiley & Sons. Copyright 2020, WILEY-VCH Verlag GmbH & Co. KGaA, Weinheim. (d)-(i) A schematic diagram of the mechano-phonic artificial synapse based on the Gr/MoS<sub>2</sub> heterostructure. (ii) A top-view SEM image of the optoelectronic transistor. (iii) Photo-activated -PSC of the artificial synapse at  $D = 1$  mm and  $P_{LED} = 3.5$  mW cm<sup>-2</sup> with light pulse width at 50 ms. From [40]. Reprinted with permission from AAAS.

conductance in InSe channels is similar to the synaptic weight ( $\Delta W$ ); thus, the triboelectric synaptic device can successfully mimic synapses learning and forgetting behavior.

Mechanoplastic FETs can be used to construct reconfigurable artificial synapses, and by further engineering the amplitude and duration, the synaptic plasticity can be simulated. As shown in figure 10(b)-(i), the tribotronic FET consists of a van der Waals (vdW) heterostructure of Gr/h-BN/WSe<sub>2</sub> and an integrated TENG device in contact-separation mode [71]. One tribo-layer of the TENG device is composed of Cu coupled to the FET gate, and the other mobile tribo-layer is composed of FEP/Cu. Half of the WSe<sub>2</sub> conducting channels are distributed vertically on the graphite flakes, forming a semi-floating-gate

FET structure. Moreover, the Gr layer acts as the FET device floating gate with the Si as the control gate, and the h-BN and SiO<sub>2</sub> act as the tunneling barrier and blocking dielectrics, respectively. To verify the feasibility of precise regulation on the synaptic FETs by mechanical displacement, the output characteristics of a tribotronic vdW transistor were tested (figure 10(b)-(ii)). The positive triboelectric potential generated by the contact separation between the TENG tribo-layers is used as the input pulse to trigger a presynaptic spike with a pulse width of 0.2 s. Due to the equivalent gate voltage coupling to the bottom gate and the inherent n-doping properties of WSe<sub>2</sub>, a momentary current pulse occurs. After removal of the input pulse, the IPSCs decreased significantly and tended to reach a steady level similar to the coherent PSCs induced by inhibitory neurotransmitter release. In contrast, when a negative triboelectric potential input pulse is applied, corresponding EPSCs are induced. Therefore, the positive and negative triboelectric potential regulation by the TENG component can ideally simulate inhibitory and excitatory behavior.

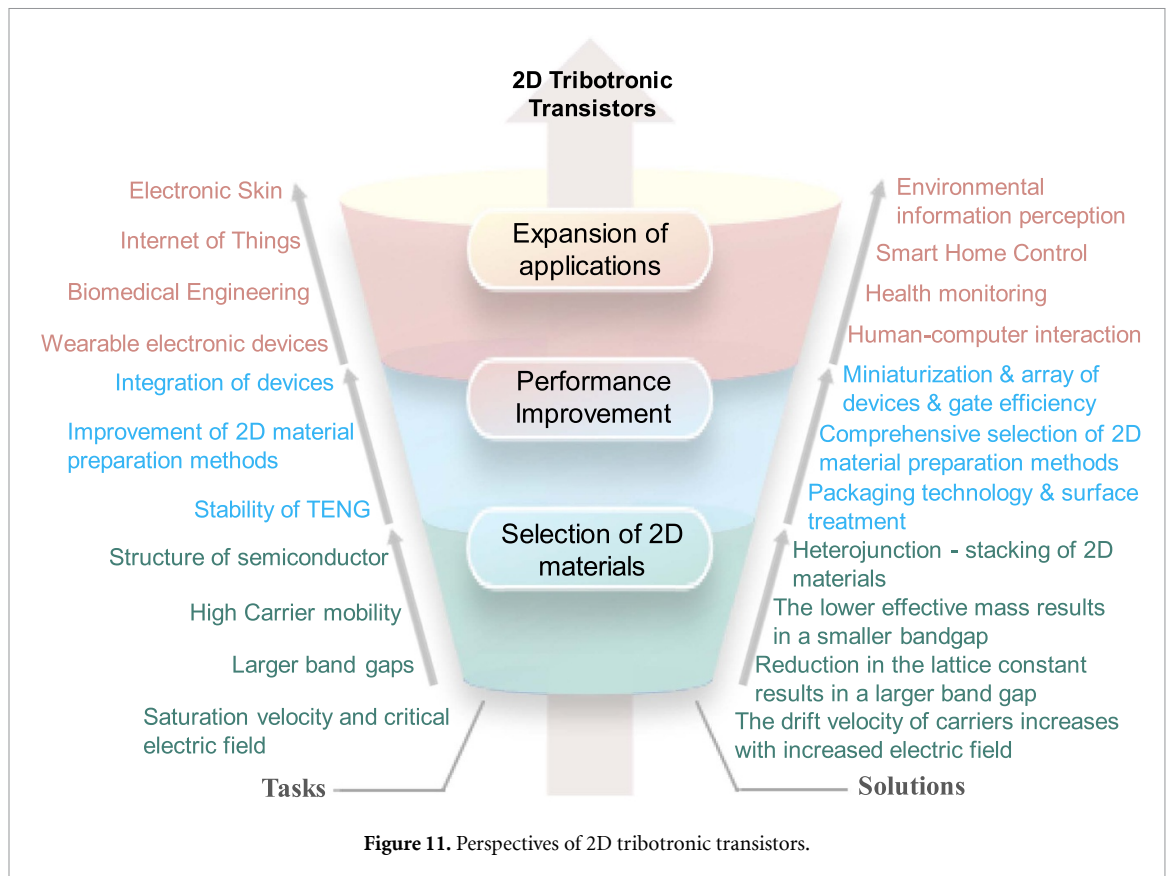
The TENG mechanical displacement can readily induce triboelectric potential to couple with the floating-gate synaptic FETs, trigger PSC signals, and modulate synaptic weight, thus successfully achieving mechanical synaptic plasticity. Yang *et al* reported a tribotronic neuromorphic FET device based on 2D materials (figure 10(c)-(i)) [72]. The CVD-grown MoS<sub>2</sub> was transferred and patterned as the FET channel, and the Au nanoparticles (as the floating-gate layer) were thermally deposited between the SiO<sub>2</sub> dielectric layer and HfO<sub>2</sub> tunneling layer. The fabricated MoS<sub>2</sub> floating-gate FET and the TENG composed of two friction layers of FEP and Cu are integrated into a mechanically regulated synaptic FET device. As shown in figure 10(c)-(ii), during the coupling of the triboelectric potentials (generated between the TENG tribo-layers) and the MoS<sub>2</sub> channel, the induced charge carriers are captured by the Au nanoparticle floating-gate layer and are gradually released through tunneling, thereby simulating the transmission of the neurotransmitter. As a result of the charge trapping of floating gates, artificial synapses can achieve both short-term and long-term plasticity derived from the mechanical displacement, providing a new development idea and directions for neuromorphic computing and potential neural system learning.

To modulate the tribotronic FETs more accurately, bimodal (or multimodal) regulation has attracted considerable attention. Yu *et al* reported a mechano-photonic multimodal artificial synapse device based on the 2D Gr/MoS<sub>2</sub> heterostructure and integrated TENG (figure 10(d)-(i)) [40]. The CVD-grown monolayer-Gr is stacked on multilayer MoS<sub>2</sub> flakes on a Si/SiO<sub>2</sub> substrate (figure 10(d)-(ii)). In the contact-separation mode TENG component, one friction layer PTFE/Cu is connected to the FET gate, while a Cu electrode acts as the other movable friction layer. In the heterostructures, the photogenerated carriers in the MoS<sub>2</sub> are transferred to Gr, and the interfacial barrier prevents the rapid recombination of photogenerated electron-hole pairs and leads to sustained photoconductivity; thus, it is beneficial to simulate the decay behavior of the biological synapses. The mechanical displacement ( $D$ ) between the two tribo-layers of the TENG can induce the triboelectric potential coupling to the FET, directly affect the charge transfer in the FET channel, and modulate the photocurrent of the synaptic devices. As shown in figure 10(d)(iii), taking  $D$  maintained at 1 mm as an instant, when the whole device was irradiated with green light pulses, the light-activated PSC showed an apparent negative increase, and when the light was turned off, the peak current gradually decreased and tended to a stable level. Therefore, in synaptic devices, the modulation behavior of triboelectric potential and photonic input synergistically affects postsynaptic excitation and inhibition. Through further simulation of artificial neural networks, the feasibility of mechanical plasticization to improve the image recognition accuracy was verified, instructing the development of multifunctional neuromorphic devices and artificial intelligence.

## 5. Summary and perspectives

This paper reviews the electrical, optoelectronic, and piezoelectric properties of typical 2D materials. Meanwhile, both the microscale and macroscale control principles of the tribotronic transistors are given in detail. In addition, the application of tribotronic FETs in different fields, such as intelligent sensors, logic devices, memory devices, and artificial synapses, is summarized. The 2D materials exhibit excellent properties of rich valence band structures and tunable thickness, showing great potential in various functional tribotronic transistors. Simultaneously, the triboelectric potential regulation can replace the FET's conventional gate voltage and effectively modulate the carrier transport characteristics in the semiconductor channel. After years of research, 2D FETs have achieved rapid development. The members of the 2D material family will continue to expand with gradually emerging new 2D semiconductor materials, which promises abundant research points and huge potential in 2D tribotronic transistors. However, challenges and opportunities coexist. To achieve higher performance and more practical tribotronic devices, different aspects need to be considered (figure 11).

In recent years, research on tribotronic transistors has received extensive attention since the new field of coupling between tribotronics and semiconductors was proposed. From the first device that introduced 2D



material optoelectronic technology into the field of tribotronics [36] to recent investigation of different 2D materials or methods on improving the device performance and expanding the applications, it is a significant indicator of the utilization of 2D materials in the continuous exploration and development of tribotronic transistors. Although many discovered 2D materials have excellent properties, their practical applications are still limited by the disadvantages of poor environmental stability, unsustainable performance after device fabrication, and high cost [124]. Therefore, appropriate 2D materials should be selected as the channel materials of FETs to achieve the desired performances. The lattice constant, bandgap, carrier mobility, and saturation velocity of 2D materials can be used as important parameters to select 2D materials. After determining the appropriate channel materials for devices, it is necessary to consider the preparation method of 2D materials, figures of merit, and the entire 2D triboelectric FET system to improve the overall performance of the integrated devices. More detailed suggestions on the development of 2D tribotronic FETs are listed from the following aspects.

- (a) 2D material selection. Elaborate selection of suitable 2D materials plays an important role in the fabrication of tribotronic transistors. First, 2D materials can be preserved, even under the atomic layer thickness, due to their unique intrinsic properties. Atomic thin 2D materials are stacked together to form vdW heterostructures, which can achieve novel properties that are different from ordinary structures. Therefore, we suggest that the heterostructures formed by 2D material stacking can be used as the channel materials of the tribotronic FET to achieve better device characteristics. In 2D semiconductor materials, a reduction in the lattice constant usually results in a larger bandgap. For example, the bandgap in TMDs decreases gradually with the increased trend of the lattice constant  $\text{MoS}_2 > \text{MoSe}_2 > \text{MoTe}_2$  [20]. This trend can help one to rapidly select from the 2D material libraries for desired bandgaps and properties to fabricate corresponding tribotronic transistors. Among all the 2D materials, the non-zero bandgap 2D materials based on Ge or Si are preferentially applied to photodetection, and are commonly the first choice for the preparation of phototransistors. Mobility is an important physical quantity that marks the speed of the movement of charge carriers under the action of an electric field, and its magnitude directly affects the operating frequency and speed of semiconductor devices and circuits [125]. The improvement in carrier mobility can optimize the potential properties of the semiconductor materials and device structures to improve the performance of semiconductor devices. Compared with other materials, 2D materials have higher carrier mobility, which can improve the output of the device [126]. Therefore, to fabricate high-performance tribotronic

transistors, the charge carrier mobility of a 2D material is another important parameter to be considered. Smaller effective mass generally results in higher carrier mobility. In addition, the lower effective mass results in a smaller bandgap, and thus the device exhibits larger off-state leakage current [127]. Therefore, an appropriate balance should be considered when selecting suitable 2D materials, and plays an important role in improving the overall output performance of tribotronic transistors. Among the different 2D semiconductor materials, MoS<sub>2</sub>, WSe<sub>2</sub>, and WS<sub>2</sub> have been widely used due to their large bandgap and relatively high carrier mobility [128]. In addition, the average drift velocity of carriers increases with the increased electric field. When the electric field increases to a certain extent (critical electric field), the drift velocity of carriers reaches a saturation value [129]. Commonly, the switching speed of the tribotronic transistor is more dependent on the saturation speed. Therefore, the saturation speed of the carrier drift and the critical electric field have a significant impact on the performance of the tribotronic transistor. The maximum saturation velocity of Gr is  $6 \times 10^7$  cm s<sup>-1</sup> [130], and some BPs exhibit  $10^7$  cm s<sup>-1</sup> [131]. Therefore, the saturation velocity parameter should also be considered when selecting 2D materials.

- (b) Device performance improvement. Improving the performance of 2D tribotronic transistors is also critical for researchers to consider. Firstly, the 2D tribotronic transistor is composed of a TENG and an FET based on 2D materials; therefore, it is necessary to consider the development toward miniaturization and device arrays. In addition, analogous to the figure of merit for conventional transistors, gating efficiency metrics of tribotronic transistors are critical to identify high-performance operations. Therefore, the integrated devices also require higher tribotronic conductivity ( $g_t$ ), a smaller threshold value ( $D_T$ ), and a steeper threshold swing ( $SS_t$ ). Secondly, the preparation process of 2D materials is very important for the improvement of device performance. Mechanical exfoliation is the simplest method used to exfoliate 2D crystal materials to obtain 2D material nanosheets [132]. The CVD method has great potential for the preparation of 2D material nanosheets. The 2D crystal materials prepared by this method have the advantages of controllable size and thickness, and excellent electrical properties. But the CVD method makes it difficult to precisely control the stoichiometric ratio, and this method has high costs and low yield [133]. In general, the existing methods for preparing 2D materials have both advantages and disadvantages; therefore, they need to be selected based on demand. The 2D tribotronic transistor integrates a TENG and an FET based on 2D channel material; therefore, further improving the stability of the TENG will greatly help to improve the performance of the whole system. As a substitute for a traditional gate voltage, the TENG plays a very important role in the whole 2D triboelectric FET system. The packaging technology can prevent the TENG from being affected by the environment and can improve its stability in the environment. In addition, surface treatment of the TENG device, such as chemical doping or surface modification, can improve the hydrophobicity of the surface to avoid performance degradation in a humid environment.
- (c) Application extension. The 2D tribotronic transistors have been proven to be applied in different directions, such as smart sensors, memories, logic devices, and artificial synapses. Considering the exciting progress of 2D FETs with regard to material synthesis, device fabrication, etc, triboelectric potential-controlled 2D FETs can be further developed into more active and intelligent sensors for environmental information perception, IoTs for smart home control, biomedical engineering for health monitoring, and wearable electronic devices for human–computer interaction.

In summary, with the continuous research and discovery of novel 2D materials, the performance of FETs will achieve new breakthroughs. Moreover, with the continuous improvements in the structure and materials of TENGs, the 2D tribotronic transistor is a highly promising candidate for application to the new generation of semiconductor devices, mechano-memory/logic-gates/microprocessors, the human–machine interface, intelligent artificial skins/neurons, and so on.

### Data availability statement

All data that support the findings of this study are included within the article (and any supplementary files).

### Acknowledgments

This work is financially supported by the National Key Research and Development Program of China (2021YFB3200304), the National Natural Science Foundation of China (52073031), Beijing Nova Program (Z191100001119047, Z211100002121148), Fundamental Research Funds for the Central Universities (E0EG6801X2), and the ‘Hundred Talents Program’ of the Chinese Academy of Sciences.

## Conflict of interest

There are no conflicts to declare.

## ORCID iDs

Jinran Yu  <https://orcid.org/0000-0003-0592-0263>

Zhong Lin Wang  <https://orcid.org/0000-0002-5530-0380>

Qijun Sun  <https://orcid.org/0000-0003-2130-7389>

## References

- [1] Penev E S, Marzari N and Yakobson B I 2021 Theoretical prediction of two-dimensional materials, behavior, and properties *ACS Nano* **15** 5959–76
- [2] Liang J et al 2022 Recent advances in nanostructured heterogeneous catalysts for N-cycle electrocatalysis *Nano Res. Energy* **1** e9120010
- [3] Safaei J and Wang G 2022 Progress and prospects of two-dimensional materials for membrane-based osmotic power generation *Nano Res. Energy* **1** e9120008
- [4] Seol M, Kim S, Cho Y, Byun K-E, Kim H, Kim J, Kim S K, Kim S-W, Shin H-J and Park S 2018 Triboelectric series of 2D layered materials *Adv. Mater.* **30** e1801210
- [5] Zhang M and Yuan J 2022 Graphene meta-aerogels: when sculpture aesthetic meets 1D/2D composite materials *Nano Res. Energy* **1** e9120035
- [6] Lin Z, Luo P, Zeng W, Lai H, Xie W, Deng W and Luo Z 2020 Improvement of photoelectric properties of MoS<sub>2</sub>/WS<sub>2</sub> heterostructure photodetector with interlayer of Au nanoparticles *Opt. Mater.* **108** 110191
- [7] Guo Z et al 2017 Metal-ion-modified black phosphorus with enhanced stability and transistor performance *Adv. Mater.* **29** 1703811
- [8] Musah J-D, Ilyas A M, Venkatesh S, Mensah S, Kwofie S, Roy V A L and Wu C-M L 2022 Isovalent substitution in metal chalcogenide materials for improving thermoelectric power generation—A critical review *Nano Res. Energy* **1** 9120034
- [9] Liang G, Li X, Wang Y, Yang S, Huang Z, Yang Q, Wang D, Dong B, Zhu M and Zhi C 2022 Building durable aqueous K-Ion capacitors based on MXene family *Nano Res. Energy* **1** e9120002
- [10] Guo X et al 2022 Vacancy manipulating of molybdenum carbide MXenes to enhance Faraday reaction for high performance lithium-ion batteries *Nano Res. Energy* **1** e9120026
- [11] Ye H and Li Y 2022 Towards practical lean-electrolyte Li–S batteries: highly solvating electrolytes or sparingly solvating electrolytes *Nano Res. Energy* **1** e9120012
- [12] Wang Z L and Song J 2006 Piezoelectric nanogenerators based on zinc oxide nanowire arrays *Science* **312** 242–6
- [13] Fan F-R, Tian Z-Q and Lin Wang Z 2012 Flexible triboelectric generator *Nano Energy* **1** 328–34
- [14] Wang Z L 2014 Triboelectric nanogenerators as new energy technology and self-powered sensors—principles, problems and perspectives *Faraday Discuss.* **176** 447–58
- [15] Wang Z L 2017 On Maxwell's displacement current for energy and sensors: the origin of nanogenerators *Mater. Today* **20** 74–82
- [16] Zou H et al 2019 Quantifying the triboelectric series *Nat. Commun.* **10** 1427
- [17] Zheng J et al 2022 Self-assembled monolayer enabling improved buried interfaces in blade-coated perovskite solar cells for high efficiency and stability *Nano Res. Energy* **1** e9120004
- [18] Wang S, Ma J, Shi X, Zhu Y and Wu Z-S 2022 Recent status and future perspectives of ultracompact and customizable micro-supercapacitors *Nano Res. Energy* **1** e9120018
- [19] Dai C, Liu Y and Wei D 2022 Two-dimensional field-effect transistor sensors: the road toward commercialization *Chem. Rev.* **122** 10319–92
- [20] Liu Y, Duan X, Shin H-J, Park S, Huang Y and Duan X 2021 Promises and prospects of two-dimensional transistors *Nature* **591** 43–53
- [21] Andrews K, Bowman A, Rijal U, Chen P-Y and Zhou Z 2020 Improved contacts and device performance in MoS<sub>2</sub> transistors using a 2D semiconductor interlayer *ACS Nano* **14** 6232–41
- [22] Hua Q et al 2020 Atomic threshold-switching enabled MoS<sub>2</sub> transistors towards ultralow-power electronics *Nat. Commun.* **11** 6207
- [23] Xue H, Gong H, Yamauchi Y, Sasaki T and Ma R 2022 Photo-enhanced rechargeable high-energy-density metal batteries for solar energy conversion and storage *Nano Res. Energy* **1** e9120007
- [24] Zhang C, Tang W, Zhang L, Han C and Wang Z L 2014 Contact electrification field-effect transistor *ACS Nano* **8** 8702–9
- [25] Zhang C, Zhang L M, Tang W, Han C B and Wang Z L 2015 Tribotronic logic circuits and basic operations *Adv. Mater.* **27** 3533–40
- [26] Xi F, Pang Y, Li W, Bu T, Zhao J, Liu G, Guo T, Liu W and Zhang C 2018 Tribotronic bipolar junction transistor for mechanical frequency monitoring and use as touch switch *Microsyst. Nanoeng.* **4** 25
- [27] Zhang C, Li J, Han C B, Zhang L M, Chen X Y, Wang L D, Dong G F and Wang Z L 2015 Organic tribotronic transistor for contact-electrification-gated light-emitting diode *Adv. Funct. Mater.* **25** 5625–32
- [28] Zhao L, Chen K, Yang F, Zheng M, Guo J, Gu G, Zhang B, Qin H, Cheng G and Du Z 2019 The novel transistor and photodetector of monolayer MoS<sub>2</sub> based on surface-ionic-gate modulation powered by a triboelectric nanogenerator *Nano Energy* **62** 38–45
- [29] Zhang S et al 2022 The self-powered artificial synapse mechanotactile sensing system by integrating triboelectric plasma and gas-ionic-gated graphene transistor *Nano Energy* **91** 106660
- [30] Sun Q, Seung W, Kim B J, Seo S, Kim S W and Cho J H 2015 Active matrix electronic skin strain sensor based on piezopotential-powered graphene transistors *Adv. Mater.* **27** 3411–7
- [31] Zhao J, Guo H, Pang Y K, Xi F, Yang Z W, Liu G, Guo T, Dong G, Zhang C and Wang Z L 2017 Flexible organic tribotronic transistor for pressure and magnetic sensing *ACS Nano* **11** 11566–73
- [32] Pang Y, Li J, Zhou T, Yang Z, Luo J, Zhang L, Dong G, Zhang C and Wang Z L 2017 Flexible transparent tribotronic transistor for active modulation of conventional electronics *Nano Energy* **31** 533–40
- [33] Bardeen J and Brattain W H 1948 The transistor, a semi-conductor triode *Phys. Rev.* **74** 230–1

- [34] Peng W, Yu R, He Y and Wang Z L 2016 Theoretical study of triboelectric-potential gated/driven metal-oxide-semiconductor field-effect transistor *ACS Nano* **10** 4395–402
- [35] Shen J, Li B, Yang Y, Yang Z, Liu X, Lim K-C, Chen J, Ji L, Lin Z-H and Cheng J 2022 Application, challenge and perspective of triboelectric nanogenerator as micro-nano energy and self-powered biosystem *Biosens. Bioelectron.* **216** 114595
- [36] Pang Y, Xue F, Wang L, Chen J, Luo J, Jiang T, Zhang C and Wang Z L 2016 Tribotronic enhanced photoresponsivity of a MoS<sub>2</sub> phototransistor *Adv. Sci.* **3** 1500419
- [37] Gao G, Wan B, Liu X, Sun Q, Yang X, Wang L, Pan C and Wang Z L 2018 Tunable tribotronic dual-gate logic devices based on 2D MoS<sub>2</sub> and black phosphorus *Adv. Mater.* **30** e1705088
- [38] Yu J, Qin S, Zhang H, Wei Y, Zhu X, Yang Y and Sun Q 2021 Fiber-shaped triboiontronic electrochemical transistor *Research* **2021** 9840918
- [39] Yu J, Gao G, Huang J, Yang X, Han J, Zhang H, Chen Y, Zhao C, Sun Q and Wang Z L 2021 Contact-electrification-activated artificial afferents at femtojoule energy *Nat. Commun.* **12** 1581
- [40] Yu J, Yang X, Gao G, Xiong Y, Wang Y, Han J, Chen Y, Zhang H, Sun Q and Wang Z L 2021 Bioinspired mechano-photonic artificial synapse based on graphene/MoS<sub>2</sub> heterostructure *Sci. Adv.* **7** eabd9117
- [41] Tan F, Xiong Y, Yu J, Wang Y, Li Y, Wei Y, Sun J, Xie X, Sun Q and Wang Z L 2021 Triboelectric potential tuned dual-gate IGZO transistor for versatile sensory device *Nano Energy* **90** 106617
- [42] Meng Y, Gao G and Zhu J 2021 Self-powered bifunctional sensor based on tribotronic planar graphene transistors *Sci. Rep.* **11** 21483
- [43] Qu W, Liu W, Li X and Wang X 2017 A triboelectric charge top-gated graphene transistor *Diam. Relat. Mater.* **73** 33–38
- [44] Xue F, Chen L, Wang L, Pang Y, Chen J, Zhang C and Wang Z L 2016 MoS<sub>2</sub> Tribotronic transistor for smart tactile switch *Adv. Funct. Mater.* **26** 2104–9
- [45] Li M et al 2019 Low-voltage operational, low-power consuming, and high sensitive tactile switch based on 2D layered InSe tribotronics *Adv. Funct. Mater.* **29** 1809119
- [46] Jia M et al 2021 Multibit tribotronic nonvolatile memory based on van der Waals heterostructures *Nano Energy* **83** 105785
- [47] Zhao J, Bu T, Zhang X, Pang Y, Li W, Zhang Z, Liu G, Wang Z L and Zhang C 2020 Intrinsically stretchable organic-tribotronic-transistor for tactile sensing *Research* **2020** 1398903
- [48] Xu L, Zhou W, Liu W, Xia X, Liu G, Guo T, Hu Z, Li Z and Zhang S 2022 Unexpected band gap evolution and high carrier mobility sparked by the orbital variation in two-dimensional GaGeX (X = S, Se, Te) *Physica E* **138** 115112
- [49] Cheng J, Wang C, Zou X and Liao L 2019 Recent advances in optoelectronic devices based on 2D materials and their heterostructures *Adv. Opt. Mater.* **7** 654
- [50] Duerloo K-A N, Ong M T and Reed E J 2012 Intrinsic piezoelectricity in two-dimensional materials *J. Phys. Chem. Lett.* **3** 2871–6
- [51] Cao Y X, Zhao C, Liu Z J, Chen X P, Mitrovic I Z, Liu Y N, Yang L, van Zalinge H and Zhao C Z 2022 Bionic artificial synaptic floating gate transistor based on MXene *Solid State Electron.* **192** 108257
- [52] Yu R, Zhang X, Gao C, Li E, Yan Y, Hu Y, Chen H, Guo T and Wang R 2022 Low-voltage solution-processed artificial optoelectronic hybrid-integrated neuron based on 2D MXene for multi-task spiking neural network *Nano Energy* **99** 104718
- [53] Ye K et al 2020 High-performance broadband photodetectors of heterogeneous 2D inorganic molecular Sb<sub>2</sub>O<sub>3</sub>/monolayer MoS<sub>2</sub> crystals grown via chemical vapor deposition *Adv. Opt. Mater.* **8** 2000168
- [54] Wu W et al 2014 Piezoelectricity of single-atomic-layer MoS<sub>2</sub> for energy conversion and piezotronics *Nature* **514** 470–4
- [55] Noor S L, Safa S and Khan M Z R 2017 A silicon-based dual-material double-gate tunnel field-effect transistor with optimized performance *Int. J. Numer. Model.: Electron. Netw. Devices Fields* **30** e2220
- [56] Cong C, Shang J, Wang Y and Yu T 2018 Optical properties of 2D semiconductor WS<sub>2</sub> *Adv. Opt. Mater.* **6** 1700767
- [57] Gao G, Yu J, Yang X, Pang Y, Zhao J, Pan C, Sun Q and Wang Z L 2019 Triboiontronic transistor of MoS<sub>2</sub> *Adv. Mater.* **31** e1806905
- [58] Lin S, Xu L, Xu C, Chen X, Wang A C, Zhang B, Lin P, Yang Y, Zhao H and Wang Z L 2019 Electron transfer in nanoscale contact electrification: effect of temperature in the metal-dielectric case *Adv. Mater.* **31** e1808197
- [59] Kim S, Kim T Y, Lee K H, Kim T-H, Cimini F A, Kim S K, Hinchet R, Kim S-W and Falconi C 2017 Rewritable ghost floating gates by tunnelling triboelectrification for two-dimensional electronics *Nat. Commun.* **8** 15891
- [60] Bu T, Xu L, Yang Z, Yang X, Liu G, Cao Y, Zhang C and Wang Z L 2020 Nanoscale triboelectrification gated transistor *Nat. Commun.* **11** 1054
- [61] Ajayan J, Nirmal D, Prajooon P and Charles Pravin J 2017 Analysis of nanometer-scale InGaAs/InAs/InGaAs composite channel MOSFETs using high-K dielectrics for high speed applications *AEU-Int. J. Electron. Commun.* **79** 151–7
- [62] Wang J, Cai Q, Lei J, Yang G, Xue J, Chen D, Liu B, Lu H, Zhang R and Zheng Y 2019 Performance of monolayer blue phosphorene double-gate MOSFETs from the first principles *ACS Appl. Mater. Interfaces* **11** 20956–64
- [63] Yin Y, Shao C, Zhang C, Zhang Z, Zhang X, Robertson J and Guo Y 2020 Anisotropic transport property of antimonene MOSFETs *ACS Appl. Mater. Interfaces* **12** 22378–86
- [64] Roy D and Biswas A 2021 Design and analysis of ultra-thin dielectric film embedded nanoscale double-gate MOSFETs for boosting logic performance *AEU-Int. J. Electron. Commun.* **131** 153614
- [65] Yang X, Han J, Yu J, Chen Y, Zhang H, Ding M, Jia C, Sun J, Sun Q and Wang Z L 2020 Versatile triboiontronic transistor via proton conductor *ACS Nano* **14** 8668–77
- [66] Zhang C and Wang Z L 2016 Tribotronics—a new field by coupling triboelectricity and semiconductor *Nano Today* **11** 521–36
- [67] Khan U, Kim T H, Ryu H, Seung W and Kim S W 2017 Graphene tribotronics for electronic skin and touch screen applications *Adv. Mater.* **29** 1603544
- [68] Zhao J, Wei Z, Yang X, Zhang G and Wang Z 2021 Mechanoplastic tribotronic two-dimensional multibit nonvolatile optoelectronic memory *Nano Energy* **82** 105692
- [69] Khan U, Kim T-H, Khan M A, Kim J, Falconi C and Kim S-W 2020 Zero-writing-power tribotronic MoS<sub>2</sub> touch memory *Nano Energy* **75** 104936
- [70] Gao C et al 2022 Touch-modulated van der Waals heterostructure with self-writing power switch for synaptic simulation *Nano Energy* **91** 106659
- [71] Jia M, Guo P, Wang W, Yu A, Zhang Y, Wang Z L and Zhai J 2022 Tactile tribotronic reconfigurable p-n junctions for artificial synapses *Sci. Bull.* **67** 803–12
- [72] Yang X, Yu J, Zhao J, Chen Y, Gao G, Wang Y, Sun Q and Wang Z L 2020 Mechanoplastic tribotronic floating-gate neuromorphic transistor *Adv. Funct. Mater.* **30** 2002506
- [73] Yu J, Yang X and Sun Q 2020 Piezo/tribotronics toward smart flexible sensors *Adv. Intell. Syst.* **2** 896

- [74] Huo Z, Peng Y, Zhang Y, Gao G, Wan B, Wu W, Yang Z, Wang X and Pan C 2018 Recent advances in large-scale tactile sensor arrays based on a transistor Matrix *Adv. Mater. Interfaces* **5** 1801061
- [75] Zhao J, Li N, Yu H, Wei Z, Liao M, Chen P, Wang S, Shi D, Sun Q and Zhang G 2017 Highly sensitive MoS<sub>2</sub> humidity sensors array for noncontact sensation *Adv. Mater.* **29** 1702076
- [76] Luo Y, Zhao T, Dai Y, Li Q and Fu H 2021 Flexible nanosensors for non-invasive creatinine detection based on triboelectric nanogenerator and enzymatic reaction *Sens. Actuators A* **320** 112585
- [77] Cao Y, Guo Y, Chen Z, Yang W, Li K, He X and Li J 2022 Highly sensitive self-powered pressure and strain sensor based on crumpled MXene film for wireless human motion detection *Nano Energy* **92** 106689
- [78] Zhao L, Wang L, Zheng Y, Zhao S, Wei W, Zhang D, Fu X, Jiang K, Shen G and Han W 2021 Highly-stable polymer-crosslinked 2D MXene-based flexible biocompatible electronic skins for *in vivo* biomonitoring *Nano Energy* **84** 105921
- [79] Luo Y, Xiao X, Chen J, Li Q and Fu H 2022 Machine-learning-assisted recognition on bioinspired soft sensor arrays *ACS Nano* **16** 6734–43
- [80] Luo Y, Wang Z, Wang J, Xiao X, Li Q, Ding W and Fu H Y 2021 Triboelectric bending sensor based smart glove towards intuitive multi-dimensional human-machine interfaces *Nano Energy* **89** 106330
- [81] Cao Y, Bu T, Fang C, Zhang C, Huang X and Zhang C 2020 High-resolution monolithic integrated tribotronic InGaZnO thin-film transistor array for tactile detection *Adv. Funct. Mater.* **30** 2002613
- [82] Kufer D and Konstantos G 2016 Photo-FETs: phototransistors enabled by 2D and 0D nanomaterials *ACS Photonics* **3** 2197–210
- [83] Zhang C, Zhang Z H, Yang X, Zhou T, Han C B and Wang Z L 2016 Tribotronic phototransistor for enhanced photodetection and hybrid energy harvesting *Adv. Funct. Mater.* **26** 2554–60
- [84] Li B, Li Z, Wu X and Zhu Z 2022 Interface functionalization in inverted perovskite solar cells: from material perspective *Nano Res. Energy* **1** e9120011
- [85] Meng Y, Zhao J, Yang X, Zhao C, Qin S, Cho J H, Zhang C, Sun Q and Wang Z L 2018 Mechanosensation-active matrix based on direct-contact tribotronic planar graphene transistor array *ACS Nano* **12** 9381–9
- [86] Zhang H, Yu J, Yang X, Gao G, Qin S, Sun J, Ding M, Jia C, Sun Q and Wang Z L 2020 Ion gel capacitively coupled tribotronic gating for multiparameter distance sensing *ACS Nano* **14** 3461–8
- [87] Wu J M, Lin Y H and Yang B-Z 2016 Force-pad made from contact-electrification poly(ethylene oxide)/InSb field-effect transistor *Nano Energy* **22** 468–74
- [88] Sun Q, Kim D H, Park S S, Lee N Y, Zhang Y, Lee J H, Cho K and Cho J H 2014 Transparent, low-power pressure sensor matrix based on coplanar-gate graphene transistors *Adv. Mater.* **26** 4735–40
- [89] Wang L et al 2018 Ultrathin piezotronic transistors with 2 nm channel lengths *ACS Nano* **12** 4903–8
- [90] Zhu J, Zhou X, Jing L, Hua Q, Hu W and Wang Z L 2019 Piezotronic effect modulated flexible AlGaN/GaN high-electron-mobility transistors *ACS Nano* **13** 13161–8
- [91] Yang Z W, Pang Y, Zhang L, Lu C, Chen J, Zhou T, Zhang C and Wang Z L 2016 Tribotronic transistor array as an active tactile sensing system *ACS Nano* **10** 10912–20
- [92] Niu S, Wang S, Lin L, Liu Y, Zhou Y S, Hu Y and Wang Z L 2013 Theoretical study of contact-mode triboelectric nanogenerators as an effective power source *Energy Environ. Sci.* **6** 3576–83
- [93] Lee Y, Kang S G and Jeong J 2021 Sliding triboelectric nanogenerator with staggered electrodes *Nano Energy* **86** 106062
- [94] Wang Z L, Lin L, Chen J, Niu S and Zi Y 2016 Triboelectric nanogenerator: single-electrode mode *Triboelectric Nanogenerators* vol 86 (Cambridge: Springer) pp 91–107
- [95] Niu S, Liu Y, Chen X, Wang S, Zhou Y S, Lin L, Xie Y and Wang Z L 2015 Theory of freestanding triboelectric-layer-based nanogenerators *Nano Energy* **12** 760–74
- [96] Han S-J et al 2017 High-speed logic integrated circuits with solution-processed self-assembled carbon nanotubes *Nat. Nanotechnol.* **12** 861–5
- [97] Michel K H and Verberck B 2009 Theory of elastic and piezoelectric effects in two-dimensional hexagonal boron nitride *Phys. Rev. B* **80** 224301
- [98] Wu W, Wei Y and Wang Z L 2010 Strain-gated piezotronic logic nanodevices *Adv. Mater.* **22** 4711–5
- [99] Zhang K, Meng D, Bai F, Zhai J and Wang Z L 2020 Photon-memristive system for logic calculation and nonvolatile photonic storage *Adv. Funct. Mater.* **30** 2002945
- [100] Lin S, Chen X and Wang Z L 2022 Contact electrification at the liquid-solid interface *Chem. Rev.* **122** 5209–32
- [101] Zhang L M, Yang Z W, Pang Y K, Zhou T, Zhang C and Wang Z L 2017 Tribotronic triggers and sequential logic circuits *Nano Res.* **10** 3534–42
- [102] Tian C, Wei L, Li Y and Jiang J 2021 Recent progress on two-dimensional neuromorphic devices and artificial neural network *Curr. Appl. Phys.* **31** 182–98
- [103] Lin P, Pan C and Wang Z L 2018 Two-dimensional nanomaterials for novel piezotronics and piezophototronics *Mater. Today Nano* **4** 17–31
- [104] Lin S, Xu L, Chi Wang A and Wang Z L 2020 Quantifying electron-transfer in liquid-solid contact electrification and the formation of electric double-layer *Nat. Commun.* **11** 399
- [105] Iqbal M W, Firdous F, Manzoor M, Ateeq H, Azam S, Aftab S, Kamran M A, Rehman A U and Majid A 2020 Study of electrical attributes of molybdenum ditelluride (MoTe<sub>2</sub>) FET using experimental and theoretical evidences *Microelectron. Eng.* **230** 111365
- [106] Kim S, Choi Y J, Woo H J, Sun Q, Lee S, Kang M S, Song Y J, Wang Z L and Cho J H 2018 Piezotronic graphene barristor: efficient and interactive modulation of Schottky barrier *Nano Energy* **50** 598–605
- [107] Lin S, Xu L, Tang W, Chen X and Wang Z L 2019 Electron transfer in nano-scale contact electrification: atmosphere effect on the surface states of dielectrics *Nano Energy* **65** 103956
- [108] Wachter S, Polyushkin D K, Bethge O and Mueller T 2017 A microprocessor based on a two-dimensional semiconductor *Nat. Commun.* **8** 14948
- [109] Liu Q et al 2022 All-in-one metal-oxide heterojunction artificial synapses for visual sensory and neuromorphic computing systems *Nano Energy* **97** 107171
- [110] Liu X et al 2017 Modulation of quantum tunneling via a vertical two-dimensional black phosphorus and molybdenum disulfide p-n junction *ACS Nano* **11** 9143–50
- [111] Guo P et al 2022 Mechanical modulation of 2D electronic devices at atto-joule energy via flexotronic effect *Adv. Funct. Mater.* **11** 256
- [112] Wu P, Ameen T, Zhang H, Bendersky L A, Ilatikhameneh H, Klimeck G, Rahman R, Davydov A V and Appenzeller J 2019 Complementary black phosphorus tunneling field-effect transistors *ACS Nano* **13** 377–85

- [113] Ielmini D and Wong H S P 2018 In-memory computing with resistive switching devices *Nat. Electron.* **1** 333–43
- [114] Han X, Du W, Chen M, Wang X, Zhang X, Li X, Li J, Peng Z, Pan C and Wang Z L 2017 Visualization recording and storage of pressure distribution through a smart matrix based on the piezotronic effect *Adv. Mater.* **29** 1701253
- [115] Wu C, Kim T W, Park J H, Koo B, Sung S, Shao J, Zhang C and Wang Z L 2020 Self-powered tactile sensor with learning and memory *ACS Nano* **14** 1390–8
- [116] Luo Z-D, Zhang S, Liu Y, Zhang D, Gan X, Seidel J, Liu Y, Han G, Alexe M and Hao Y 2022 Dual-ferroelectric-coupling-engineered two-dimensional transistors for multifunctional in-memory computing *ACS Nano* **16** 3362–72
- [117] Zang Y, Zhang F, Huang D, Gao X, Di C A and Zhu D 2015 Flexible suspended gate organic thin-film transistors for ultra-sensitive pressure detection *Nat. Commun.* **6** 6269
- [118] Liu Y, Ping J and Ying Y 2021 Recent progress in 2D-nanomaterial-based triboelectric nanogenerators *Adv. Funct. Mater.* **31** 2009994
- [119] Sun Q, Ho D H, Choi Y, Pan C, Kim D H, Wang Z L and Cho J H 2016 Piezopotential-programmed multilevel nonvolatile memory as triggered by mechanical stimuli *ACS Nano* **10** 11037–43
- [120] Chen Y et al 2019 Piezotronic graphene artificial sensory synapse *Adv. Funct. Mater.* **29** 1900959
- [121] Arnold A J, Razavieh A, Nasr J R, Schulman D S, Eichfeld C M and Das S 2017 Mimicking neurotransmitter release in chemical synapses via hysteresis engineering in MoS<sub>2</sub> transistors *ACS Nano* **11** 3110–8
- [122] Liu Y, Zhong J, Li E, Yang H, Wang X, Lai D, Chen H and Guo T 2019 Self-powered artificial synapses actuated by triboelectric nanogenerator *Nano Energy* **60** 377–84
- [123] Jiang J et al 2017 2D MoS<sub>2</sub> neuromorphic devices for brain-like computational systems *Small* **13** 1700933
- [124] Khan K et al 2020 Recent developments in emerging two-dimensional materials and their applications *J. Mater. Chem. C* **8** 387–440
- [125] Feng X, Huang X, Chen L, Tan W C, Wang L and Ang K-W 2018 High mobility anisotropic black phosphorus nanoribbon field-effect transistor *Adv. Funct. Mater.* **28** 1801524
- [126] Ahmed S and Yi J 2017 Two-dimensional transition metal dichalcogenides and their charge carrier mobilities in field-effect transistors *Nano-Micro Lett.* **9** 50
- [127] Cheng L and Liu Y 2018 What limits the intrinsic mobility of electrons and holes in two dimensional metal dichalcogenides? *J. Am. Chem. Soc.* **140** 17895–900
- [128] Lee Y, Fiore S and Luisier M 2019 *Ab initio* mobility of single-layer MoS<sub>2</sub> and WS<sub>2</sub>: comparison to experiments and impact on the device characteristics *IEEE Int. Electron Devices Meeting (IEDM) 2019* pp 1–4
- [129] Li L, Yu Y, Ye G J, Ge Q, Ou X, Wu H, Feng D, Chen X H and Zhang Y 2014 Black phosphorus field-effect transistors *Nat. Nanotechnol.* **9** 372–7
- [130] Yamoah M A, Yang W, Pop E and Goldhaber-Gordon D 2017 High-velocity saturation in graphene encapsulated by hexagonal boron nitride *ACS Nano* **11** 9914–9
- [131] Chen X et al 2018 Large-velocity saturation in thin-film black phosphorus transistors *ACS Nano* **12** 5003–10
- [132] Kang K, Chen S and Yang E-H 2020 Synthesis of transition metal dichalcogenides *Synthesis, Modeling, and Characterization of 2D Materials, and Their Heterostructures* (Amsterdam: Elsevier) pp 247–64
- [133] Yabe Y, Ohtake Y, Ishitobi T, Show Y, Izumi T and Yamauchi H 2004 Synthesis of well-aligned carbon nanotubes by radio frequency plasma enhanced CVD method *Diam. Relat. Mater.* **13** 1292–5